

UCLA

UCLA Previously Published Works

Title

Injectable polypeptide hydrogels via methionine modification for neural stem cell delivery.

Permalink

<https://escholarship.org/uc/item/8t18d559>

Authors

Wollenberg, AL
O'Shea, TM
Kim, JH
[et al.](#)

Publication Date

2018-09-01

DOI

10.1016/j.biomaterials.2018.03.057

Peer reviewed

Manuscript Number: jbmt43815R1

Title: Injectable polypeptide hydrogels via methionine modification for neural stem cell delivery

Article Type: SI: Chemistry of Biomaterials

Section/Category: Biomaterials and the Stem Cell Niche (BSCN)

Keywords: biomaterials; polypeptides; hydrogels; neural stem cells; brain; cell transplantation

Corresponding Author: Dr. T.J. Deming,

Corresponding Author's Institution: UCLA

First Author: Alexander L Wollenberg

Order of Authors: Alexander L Wollenberg; Timothy M O'Shea, PhD; Jae H Kim; Anne Czechanski; Laura G Reinholdt, PhD; Michael V Sofroniew, MD, PhD; Timothy J Deming, PhD

Abstract: Injectable hydrogels with tunable physiochemical and biological properties are potential tools for improving neural stem/progenitor cell (NSPC) transplantation to treat central nervous system (CNS) injury and disease. Here, we developed injectable diblock copolypeptide hydrogels (DCH) for NSPC transplantation that contain hydrophilic segments of modified L-methionine (Met). Multiple Met-based DCH were fabricated by post-polymerization modification of Met to various functional derivatives, and incorporation of different amino acid comonomers into hydrophilic segments. Met-based DCH assembled into self-healing hydrogels with concentration and composition dependent mechanical properties. Mechanical properties of non-ionic Met-sulfoxide formulations (DCHMO) were stable across diverse aqueous media while cationic formulations showed salt ion dependent stiffness reduction. Murine NSPC survival in DCHMO was equivalent to that of standard culture conditions, and sulfoxide functionality imparted cell non-fouling character. Within serum rich environments in vitro, DCHMO was superior at preserving NSPC stemness and multipotency compared to cell adhesive materials. NSPC in DCHMO injected into uninjured forebrain remained local and, after 4 weeks, exhibited an immature astroglial phenotype that integrated with host neural tissue and acted as cellular substrates that supported growth of host-derived axons. These findings demonstrate that Met-based DCH are suitable vehicles for further study of NSPC transplantation in CNS injury and disease models.

Responses to Reviewer Comments: Ms. No. jbmt43815.

Responses given in *blue and italics*.

Reviewer #3:

This manuscript developed a new injectable modified L-methionine (Met) based diblock copolypeptide hydrogels (DCH) amenable to NSPC transplantation. The findings are novel and interesting. It's publishable.

We appreciate the reviewer's positive comments about our manuscript.

Reviewer #4:

In this study, the authors use injectable diblock copolypeptide hydrogels (DCH) for neural stem/progenitor cell (NSPC) transplantation. Although this idea and strategy is not new, the application of this paper work aims at central nervous system injury and disease are interesting.

Although the reviewer states that the idea and strategy is not new, we would like to point out that design and preparation of the DCH in this manuscript are new, and introduce a practical, efficient means to tune biomaterial hydrogel properties via a variety of different methionine modifications, which is unprecedented. Also, this manuscript introduces a new passagable NSPC line not previously described that contains transgenically inserted Ribotag functionality. The Ribotag transgene provides a transplant cell identification marker on histology (as demonstrated here) as well as the capacity to precipitate translating mRNA of only grafted cells from whole tissue in future studies. We affirm that these cells will be an important tool for us and others in the CNS grafting field moving forward and this manuscript serves an important first evaluation of their potential.

Some concerns and critical issues are listed below for the quality improvement of this paper manuscript.

1. From the data of Scheme 1, it seems like that the synthesized MA copolymer can become gelation only in very low M/A ratio (M:A=97.5:2.5). This may greatly limit its further biomedical applications.

As noted in the rationale given in the text on p.17-18, gelation in the synthesis of MA copolymers was not desired because it interferes with the ability to prepare diblock copolypeptides, and so we focused attention on the MA segment compositions that did not form gels in the organic solvent reaction mixture. Hence, the narrow window for organogel formation seen for MA compositions was not at all limiting in our subsequent preparation of hydrogels. Please note that there was no intention, or mention anywhere in the text, that these organogel reaction mixtures should be used in biomedical applications. This experiment

was used only as part of the optimization of copolypeptide synthesis en route to hydrogel preparation.

2. As shown in Scheme 2, there 's a Ala in the backbone chemical structure of modified methionine amphiphilic diblock copolypeptides. Please specify the reason in the manuscript.

The incorporation of Ala residues in the modified methionine segments was used to facilitate synthesis of the copolypeptides, and the rationale for Ala incorporation, and its (negligible) effect on resulting modified methionine copolypeptide properties, was described in detail in the text on p. 17-18.

3. From Fig. 1A and Fig. 2A, it is not understandable why the rheological property of DCHMO hold the highest storage modulus in the condition of L28 and then drop down, while DCHMM show different pattern without such phenomenon.

This phenomenon was due to bulk copolypeptide precipitation in aqueous solution for samples with L segments greater than 28, as described in the text on p. 20-21, and shown in Table 2. Once copolypeptide precipitates, its ability to contribute to gelation of water via hydrated network formation is diminished. As stated in the text, DCH_{MM} stiffness did not decrease as much as DCM_{MO} at higher L lengths most likely due to increased solubility of the ionic MM segments vs. the non-ionic MO segments. Our data on partially ionic DCH_{MOK} samples (shown in Figure 4) support this hypothesis.

Also, in Fig. 3, it is not clear why the authors change to L24? It would be better to keep consistency for data comparison.

Samples with shorter L24 segments were used in Figures 3 and 4 since we chose these compositions for all subsequent cell and animal studies, and wanted to evaluate how these compositions behaved in ionic media, similar to how they would be used for biological experiments. The L24 samples were chosen for biological studies since their mechanical properties (e.g. stiffness) were similar to values we have previously found useful in hydrogels for central nervous system applications. This rationale for sample choice was added to the text on p.22 and 24.

4. In Fig. 5, it is not clear why the cell viability of DCHMM is lower than that in DCHMO. Is it because of cytotoxicity or other factors such as mechanical property?

The cell viability in presence of DCH_{MM} is lower due to toxicity of the cationic hydrophilic segments. This is a well known phenomenon within the literature, and we discussed this on page 24, with reference to cationic lysine based hydrogels, which are also cytotoxic. The toxicity is not due to mechanical properties, since

non-ionic DCH_{MO} of near identical composition were found to be significantly less cytotoxic.

5. Although the effects of ionic media and amino acid composition have been tested in this paper, the mechanism behind did not comprehensively discussed, investigated and addressed. The scientific impact of this study is low.

We presented and discussed the effects of amino acid composition on hydrogel formation and properties, and quantified these changes using a variety of rheology measurements (i.e. Figures 1 and 2). We also presented and discussed the effects of different, biologically relevant, ionic media on different hydrogel compositions, and quantified the effects of ionic media as a function of ionic content in the hydrogels using a variety of rheology measurements (i.e. Figures 3 and 4). We feel these detailed studies are comprehensive for the purposes of evaluating these new hydrogels for biological/biomaterial uses. We also provided discussion on interpretations of the results based on observations made in this work, as well as previous work by our lab and others on similar materials (p.20-23).

6. In Fig. 7, only in vitro 2D monolayer cell culture condition is demonstrated in this work. However, 3D model should be considered to provide more convincing evidence and potential benefits of their Met Based DCH hydrogel. Although NSPC has been transplanted into mouse, it is healthy animal model but not disease CNS model. No therapeutic potential can be evaluated based on this aspect.

The work described in Figure 7 is intended to demonstrate the influence of polypeptide hydrophilic chain properties on NSPC differentiation outcomes in a serum rich (FBS) environment. The coated substrate assay used here was deemed the best way to probe to the cellular interactions with the different polypeptide species (the various Met based DCH and gelatin) in this serum environment. Specifically, this assay set up removes the effect of any potential confounders from other properties of these different polypeptides that are present in a 3D culture such as the polypeptide concentration necessary for gelation and the porosity of the hydrogel which would both influence the extent of FBS perceived by the NSPC, which is fundamental to this assay. Based on this we affirm that the assay design was appropriate for the experimental hypothesis being tested. Towards understanding how cell suspension within a 3D hydrogel effects cell differentiation we evaluated the effect of NSPC suspension within Met based DCH by qPCR (see Supplementary Figure 10 of the original manuscript, which is now Supplementary Figure 11 in the updated manuscript) which demonstrates that the gene expression of canonical neural stem cell markers for the NSPC are unchanged after 6 hours of incubation in DCH_{MO}.

As first proof of principle in vivo experiments we transplanted NSPC loaded in DCH_{MO} into healthy, uninjured mouse brains. This is a widely accepted approach

used throughout the neural stem cell and biomaterial literature to evaluate a new neural stem cell line and/or biomaterial in order to assay biomaterial CNS compatibility, how grafted cells interact with host neural tissue, and to evaluate spontaneous differentiation outcomes of grafted cells in vivo. We affirm that this is a necessary and important first step before investigating grafting the NSPC in an injury model. We clearly articulate this point in the manuscript and we also specify in the discussion section our intent in future work to use these cells in CNS injury models.

7. In the Abstract line 46, the authors mention that DCH can assemble into hydrogels and display self-healing behavior. However, the self-healing property did not reveal in the result data.

Self-healing properties of DCH_{MO} and DCH_{MM} were described and quantified in Figure 1D and Figure 2D, respectively, as well as on p.21 in the text. Also, we have explicitly added “self-healed to recover elastic properties” for the section on DCH_{MO}, while “self-healing” was already included in the section for DCH_{MM}.

8. From the "Guides to Authors", all manuscripts are to be supplied with an abstract of about 100-200 words in length. Obviously, the abstract of this paper manuscript is 255 words, more than 200 words; thus, should be shortened.

We appreciate the reviewer’s thoroughness in evaluating the length of our abstract. We have made efforts to shorten it and have updated it within the manuscript. The abstract is now 200 words.

9. The Introduction is lengthy and can also be shortened to be more neatly and precisely.

We have shortened the introduction without distorting the important background information presented and have updated it within the manuscript.

10. The number of References is 78. The number of self-citation papers are also very high. I strongly suggest the authors to prevent over-citation of their own paper works.

We have reduced the number of self-citations by 9 and now have an overall total of 68 citations.

11. Too many abbreviations used in this manuscript (viz., K180L20, DCHK , rac-EP2, DCHEO, DCHMM , DCHMO , DCHMOK , DCH27 , MR, MO, MA170Ln, (MOA)170Ln , (MOxKy)170L23, (MMA)170Ln , Mm, MAm, MOAm, etc) making it extremely difficult for the readers to correctly understand and grasp the important points and idea of this paper work. This may distract the major focus of this study and make readers feel very confused in the jungle.

Our manuscript describes the development of new copolypeptide hydrogel precursors (based on methionine), the subsequent modification of these precursors to generate samples with different functionality, and the formulation of these copolypeptides into hydrogels. To concisely and adequately describe this large set of molecules and materials, we have developed a systematic method of nomenclature that is unambiguous and is used universally across nearly all of our publications on copolypeptides. Many of the abbreviations used here refer to abbreviations used in prior manuscripts (e.g. rac-EP2, K180L20, DCH, MO, MM, etc.), and changing them here would lead to inconsistency and confusion. We have defined all abbreviations in the text where they first appear, which is usually considered adequate.

Reviewer #5:

The manuscript describes systematic development of new hydrogels diblock copolypeptide hydrogels, which are improvement over previous work of the authors aiming for cytocompatible materials stimulating central nervous system regeneration. Overall, the manuscript is well written and contains novel work. It is based on thorough and systematic evaluation of physical properties through a range of materials, however the final in vivo work concluding the manuscript is missing important controls making it less attractive to biomaterials audience.

Authors state that the cells were subcultured over several passages. Please provide information about the passage number of NSPC used for the experiments.

NSPC stocks that had undergone 15-24 passages (5-8 weeks of neural expansion) were used for experimental studies. We performed qPCR on samples derived from NSPC across this passage range and confirmed no change in gene expression of canonical neural stem cell markers. This information has been included in the methods section of manuscript.

Page 28 line 34 - authors say that the in vivo viability of the engrafted cells is excellent. Survival is impossible to determine in vivo. Fraction of the injected cells survived, but overall viability can't be claimed as "excellent". The in vivo experiment would benefit from showing a control where mice were injected with hydrogel only to show the hydrogel specific host tissue reaction to the material, as well as cell injection alone, without the hydrogel. Without these two controls the experiment is very descriptive and does not allow for full evaluation of the hydrogel effects. Moreover, since the work aims on development of improved materials, the state-of-the-art material should be used to as a another control to determine if the changes to material chemistry resulted in the intended improvement in vivo. I strongly suggest to authors to repeat in vivo experiments with appropriate set of controls, which will allow to determine and quantify the outcomes of hydrogel/NSPC implantation.

The sentence identified by the reviewer on Page 28 line 34 in the original manuscript does not refer to the viability of the grafted NSPC as suggested by the reviewer but rather states that the viability of the host tissue (neuronal and astroglial cells) in proximity to the graft is good. We have edited the language used in this sentence to avoid any confusion on this point. It should be noted that we do not make any claims about the extent of viability of the grafted cells in the manuscript other than the fact that cells did survive in sufficient numbers to easily evaluate their cellular identity and their interaction with host tissue.

The in vivo work included in this manuscript is a first proof of principle evaluation of how grafted cells interact with host neural tissue, and an evaluation of spontaneous differentiation outcomes of grafted cells in vivo using this new biomaterial/NSPC line combination.

We thank the reviewer for suggesting the inclusion of a control where mice were injected with hydrogel only to show the hydrogel specific host tissue reaction to the material. To address this we have included a new supplementary panel (now Supplementary Figure 10 in the newly updated manuscript) that compares the foreign body response of DCH_{MO} alone with a saline control in uninjured mouse brain at 1 week. DCH_{MO} alone caused minimal host CNS tissue disruption. Specifically, the proximal neuronal survival as well as the extent and magnitude of the reactive astroglial response for the DCH_{MO} was comparable to that of the saline injection.

Regarding the suggestion for a comparison with cells grafted with or without hydrogel, or comparison with other hydrogel formulations, we consider that performing a detailed study of this kind is far beyond the scope of this current manuscript which focuses on the development and characterization of this new material and NSPC line. A study of this kind requires detailed and rigorous evaluations, and we will conduct such evaluations and comparisons as a requisite demonstration for our next manuscript. Meanwhile, we attest that the work described here shows that we have an improved biomaterial in a number of ways. Specifically, the new DCH formulations allow for improved ease of synthesis, allow for improved functionalization and demonstrate more versatile physiochemical properties than other predecessor materials. These advantageous attributes of the new hydrogel are key points made within this manuscript.

Injectable polypeptide hydrogels via methionine modification for neural stem cell delivery

¹A.L. Wollenberg*, ²T.M. O'Shea*, ²J.H. Kim, ³A. Czechanski, ³L.G. Reinholdt, ²M.V. Sofroniew, and ¹T.J. Deming†.

¹ Departments of Bioengineering, Chemistry and Biochemistry, University of California, Los Angeles, Los Angeles, California 90095-1600, USA.

² Department of Neurobiology, David Geffen School of Medicine, University of California, Los Angeles, California 90095-1763, USA.

³ The Jackson Laboratory, Bar Harbor, Maine, 04609, USA.

* These authors contributed equally to this work.

† Corresponding Author

Abstract:

Injectable hydrogels with tunable physiochemical and biological properties are potential tools for improving neural stem/progenitor cell (NSPC) transplantation to treat central nervous system (CNS) injury and disease. Here, we developed injectable diblock copolypeptide hydrogels (DCH) for NSPC transplantation that contain hydrophilic segments of modified L-methionine (Met). Multiple Met-based DCH were fabricated by post-polymerization modification of Met to various functional derivatives, and incorporation of different amino acid comonomers into hydrophilic segments. Met-based DCH assembled into self-healing hydrogels with concentration and composition dependent mechanical properties. Mechanical properties of non-ionic Met-sulfoxide formulations (DCH_{MO}) were stable across diverse aqueous media while cationic formulations showed salt ion dependent stiffness reduction. Murine NSPC survival in DCH_{MO} was equivalent to that of standard culture conditions, and sulfoxide functionality imparted cell non-fouling character. Within serum rich environments *in vitro*, DCH_{MO} was superior at preserving NSPC stemness and multipotency compared to cell adhesive materials. NSPC in DCH_{MO} injected into uninjured forebrain remained local and, after 4 weeks, exhibited an immature astroglial phenotype that integrated with host neural

1
2
3
4
5
6
7
8
9
10
11
12
13
14
15
16
17
18
19
20
21
22
23
24
25
26
27
28
29
30
31
32
33
34
35
36
37
38
39
40
41
42
43
44
45
46
47
48
49
50
51
52
53
54
55
56
57
58
59
60
61
62
63
64
65

tissue and acted as cellular substrates that supported growth of host-derived axons. These findings demonstrate that Met-based DCH are suitable vehicles for further study of NSPC transplantation in CNS injury and disease models.

Keywords: biomaterials; polypeptides; hydrogels; neural stem cells; brain; cell transplantation.

1. Introduction

Transplantation of neural stem/progenitor cells (NSPC) has emerged as a potential therapy for treatment of central nervous system (CNS) diseases and injuries including Parkinson's, spinal cord injury, and stroke¹. NSPC can be readily derived from embryonic^{2,3}, adult⁴⁻⁶, and induced pluripotent stem (iPS) sources⁷ and upon transplantation *in vivo* show a capacity to differentiate into glial and neuronal phenotypes that can integrate into host circuitry^{8,9}. In the context of injury or disease, NSPC grafting has aided host neuronal survival, axon regeneration, remyelination and traumatic lesion re-vascularization¹⁰. However, despite their promise, NSPC therapies face considerable challenges including: (i) widespread cell graft necrosis and apoptosis^{11,12}, (ii) inappropriate differentiation and cell fate decision making, (iii) cellular migration away from lesioned/diseased neural tissue resulting in ectopic colonies along the brain and spinal cord neuroaxis, and (iv) isolation of cell grafts away from adjacent viable neural tissue by graft induced inflammation and fibrosis^{6,13,14}. Inability to address these challenges limits the functional potential of NSPC transplantation and hampers clinical translation. NSPC transplantation would benefit from innovative bioengineering strategies that: (1) enhance survival of injected cells; (2) direct progenitor differentiation *in vivo*; and (3) optimize graft-host interactions. Injectable hydrogel carriers have emerged as potential tools to aid NSPC transplantation. To date, fibrin gels have been the predominant material of choice in NSPC grafting studies due to their commercial availability and straight forward formulation¹⁵⁻¹⁷. However, the limited control over physical, chemical and mechanical properties of fibrin gels and their inherent and uncontrollable bioactivity has prompted efforts to develop alternative synthetic hydrogels for NSPC transplantation^{18,19}.

To identify hydrogel properties that influence NSPC transplantation outcomes we and others have been focused on engineering injectable synthetic hydrogels with robust tunability of physiochemical and biological properties. For example, blends of hyaluronan and methylcellulose have demonstrated utility in enhancing the survival of grafted NSPCs in models of spinal cord injury²⁰, retinal disease and stroke²¹. In these

1
2
3
4 studies, a rigorous mechanistic investigation uncovered a pro-survival effect of the
5 inclusion of bioactive hyaluronan, which was attributed to its high affinity for CD44
6 receptors on progenitor cells²¹. Variations in methylcellulose concentration also allowed
7 for manipulation of hydrogel mechanical properties, which influenced the injectability
8 and overall survival of transplanted NSPC using this system. Other studies using an
9 elastin-like protein based hydrogel established that the progenitor state of NSPC is
10 modulated by the stiffness and degradability of the suspending matrix²².
11
12
13
14
15
16
17
18

19 We have developed biomimetic hydrogels for drug delivery and cell transplantation
20 using synthetic polypeptides. Polypeptide hydrogels are versatile materials that can: (i)
21 be enzymatically degraded, (ii) include a wide range of chemical functionality, (iii) adopt
22 ordered conformations that can drive structural and mechanical properties, and (iv)
23 respond to biological stimuli^{1,23}. Our synthetic materials are based on amphiphilic
24 diblock copolypeptide hydrogels (DCH) that in their first iteration were composed of
25 discrete hydrophobic and ionic hydrophilic segments (e.g. poly(L-lysine-HCl)₁₈₀-*block*-
26 poly(L-leucine)₂₀, **K₁₈₀L₂₀** or DCH_K)^{24,25}, and possessed many features attractive for
27 CNS applications^{26,27}. DCH are physically associated gels composed of branched and
28 tangled nanoscale tape-like assemblies that can be deformed by applied stress and
29 injected through narrow diameter cannulae, after which they rapidly re-assemble into
30 elastic gel networks^{24,25}. When injected into mouse CNS tissues, ionic DCH self-
31 assemble into discrete, well-formed deposits of rigid gel networks *in vivo* that integrate
32 well with host CNS tissue, causing no detectable toxicity, and are fully degraded *in*
33 *vivo*²⁷. We also reported both *in vitro* and *in vivo* evidence that ionic DCH can serve as
34 depots for sustained local release of both hydrophilic and hydrophobic effector
35 molecules for investigative and potential therapeutic applications in the CNS²⁶.
36
37
38
39
40
41
42
43
44
45
46
47
48
49
50

51 Although they have many advantageous properties as hydrogels *in vivo*, one limitation
52 of ionic DCH is their cytotoxicity towards cells encapsulated completely within the
53 material matrix²⁸, which precludes their use in cell grafting applications. To obtain cell-
54 compatible hydrogels, we focused on creating non-ionic DCH, since non-ionic polymers
55 and hydrogels are well known to be less toxic to cells *in vitro*²⁹. In an initial proof of
56
57
58
59
60
61
62
63
64
65

1
2
3
4 concept study, we developed DCH containing non-ionic poly(γ -[2-(2-
5 methoxyethoxy)ethyl]-*rac*-glutamate), **rac-E^{P2}**, hydrophilic segments instead of charged
6 polypeptide segments, and found the resulting hydrogels, termed DCH_{EO}, retained the
7 advantageous physical properties of ionic DCH, as well as displayed no significant
8 cytotoxicity to either mesenchymal stem cells or NSPC for periods up to 7 days *in vitro*.
9 Furthermore, DCH_{EO} demonstrated improved cell viability, localization and host
10 integration of NSPC grafted into crush spinal cord injury lesions compared to that
11 afforded by culture media alone²⁸. The enhanced performance was attributed to
12 superior suspension of the NSPCs and a more even distribution of grafted cells within
13 the SCI lesion afforded by DCH_{EO}. While DCH_{EO} are promising as cell carriers, the
14 chemistry of the **rac-E^{P2}** component limits the further development and utility of these
15 hydrogels. In addition to being composed of unnatural amino acids that require
16 additional synthesis steps and purification, hydrolysis of side-chain linkages may lead to
17 premature degradation of the DCH_{EO} in aqueous media. The reactivity of side-chain
18 ester linkages also prohibits the incorporation of other protected functional monomers
19 into DCH_{EO}, since most deprotection conditions will also cleave off the diethylene glycol
20 chains from the glutamate residues.
21
22
23
24
25
26
27
28
29
30
31
32
33
34
35
36

37 In the study presented here, we sought to overcome the synthesis and functionality
38 limitations associated with DCH_{EO} by utilizing new methods for post-polymerization
39 modification of L-methionine (Met) residues in copolypeptides³⁰ to enable scalable
40 synthesis and add new capabilities beyond those in DCH_{EO}. Met is an essential amino
41 acid in living systems with rich biochemistry. For example, Met residues can be
42 selectively alkylated to give sulfonium salt derivatives that allow for the introduction of
43 ionic groups in polypeptides^{31,32}. This chemistry has been used to convert hydrophobic,
44 α -helical poly(L-methionine), **M**, into a wide variety of water soluble, ionic poly(S-alkyl-L-
45 methionine sulfonium)s, **M^R**, containing diverse functionality³³. Alternatively, Met
46 residues can also be readily and selectively oxidized to give highly polar, non-ionic L-
47 methionine sulfoxide, MetO, residues³⁴⁻³⁶. Polymers containing MetO residues have
48 shown interesting physiochemical and biological properties that may be advantageous
49 for their use in hydrogels for NSPC transplantation³⁷⁻⁴¹. For example, membranes of
50
51
52
53
54
55
56
57
58
59
60
61
62
63
64
65

1
2
3
4 poly(L-methionine sulfoxide), \mathbf{M}^{O} , demonstrated enhanced water permeability compared
5 to parent, non-oxidized, \mathbf{M} polymers^{37,38}, as well as improved solubility and transport of
6 hydrophilic polypeptide drugs and hydrophobic small molecules³⁹. Furthermore, \mathbf{M}^{O}
7 chains have been found to exhibit negligible diffusion across cell membranes, and
8 sulfoxide groups in polymers and on surfaces have been found to impart inherent
9 resistance against protein adsorption. The mechanism of this exceptional protein and
10 cell non-fouling character has been attributed to the capacity of sulfoxide groups to act
11 as hydrogen bond acceptors but not donors, analogous to how ethylene oxide groups
12 contribute to protein adsorption resistance in polyethylene glycol based materials⁴²⁻⁴⁴.
13 These characteristics suggest that \mathbf{M}^{O} may be an excellent component for biomaterial
14 formulations with negligible *in vitro* or *in vivo* cytotoxicity^{41,45-47}. Additionally, since
15 biological systems contain catabolic enzymatic mechanisms to readily reduce MetO
16 residues in proteins back to Met, and we have shown \mathbf{M}^{O} polymer can be readily
17 degraded by proteolytic enzymes *in vitro*⁴⁰, \mathbf{M}^{O} based biomaterials should be readily
18 and safely resorbed *in vivo*⁴⁸.
19
20
21
22
23
24
25
26
27
28
29
30
31
32

33 Given the numerous advantages described above, both alkylated and oxidized \mathbf{M} chains
34 represent potentially attractive candidates as hydrophilic segments in DCH intended for
35 use in NSPC grafting applications. The abundance and low cost of the precursor Met
36 amino acid, the ease of synthesis and purification of Met NCA monomer, and high yield
37 polymerization and post-polymerization modification reactions⁴⁹ allow the modified Met-
38 based DCH platform to be readily scalable and amenable to being manufactured in
39 compliance with GMP standards that would be required for human use. Here, we outline
40 the design and synthesis of modified Met-based DCH materials, demonstrate the
41 tunable physiochemical and biological properties achieved through post-polymerization
42 modifications of the Met residues, and establish the utility of specific formulations of
43 Met-sulfoxide based DCH_{MO} for NSPC transplantation applications.
44
45
46
47
48
49
50
51
52
53
54
55
56
57
58
59
60
61
62
63
64
65

2. Materials and Methods

2.1. Synthesis and characterization of copolypeptides

2.1.1. Materials and Instrumentation

Tetrahydrofuran (THF), hexanes, and methylene chloride were dried by purging with nitrogen and passage through activated alumina columns prior to use. Triethylamine (TEA) and trimethylsilyl chloride (TMSCl) were purified by distillation and stored over 3 Å molecular sieves. Co(PMe₃)₄, L-methionine, L-leucine, and L-alanine amino acid N-carboxyanhydride (NCA) monomers were prepared according to literature procedures^{27,49,50}. All other chemicals were purchased from commercial suppliers and used without further purification unless otherwise noted. Selecto silica gel 60 (particle size 0.032–0.063 mm) was used for flash column chromatography. Fourier Transform Infrared (FTIR) measurements were taken on a Perkin Elmer RX1 FTIR spectrophotometer calibrated using polystyrene film, and attenuated total reflectance infrared (ATR-IR) data were collected using a PerkinElmer Spectrum 100 FTIR spectrometer equipped with a universal ATR sample accessory. ¹H NMR spectra were acquired on a Bruker ARX 400 spectrometer. Tandem gel permeation chromatography/light scattering (GPC/LS) was performed at 25 °C using an SSI Accuflow Series III pump equipped with Wyatt DAWN EOS light scattering and Optilab REX refractive index detectors. Separations were achieved using 100 Å and 1000 Å PSS-PFG 7 μm columns at 30 °C with 0.5% (w/w) KTFA in 1,1,1,3,3,3-hexafluoroisopropanol (HFIP) as eluent and sample concentrations of 10 mg/ml. Pyrogen free deionized water (DI) was obtained from a Millipore Milli-Q Biocel A10 purification unit. Dialysis was conducted using regenerated cellulose dialysis tubing (Spectrum Labs).

2.1.2. Preparation of N-Boc-L-lysine NCA

The preparation of N-Boc-L-lysine NCA was modified from a procedure in literature⁵¹. To a solution of N-Boc-L-lysine amino acid (1 equiv) in dry THF (0.15 M) in a Schlenk flask was added TEA (2 equiv) and TMSCl (2 equiv) via syringe. The reaction was stirred under N₂ at 20 °C for 1 hour. Upon addition of TEA and TMSCl, precipitation of TEA·HCl was observed. Phosgene solution in toluene (15% (w/v), 2 equiv) was then

1
2
3
4 added via syringe and the reaction was stirred under N₂ at 50 °C for 2 hours. *Caution!*
5
6 Phosgene is extremely hazardous and all manipulations must be performed in a well-
7
8 ventilated chemical fume hood with proper personal protection and necessary
9
10 precautions taken to avoid exposure. After 2 hours, the reaction was evaporated to
11
12 dryness and transferred into a N₂ filled glovebox. In the fume hood, the condensate in
13
14 the Schlenk line vacuum traps was treated with 50 mL of concentrated aqueous NH₄OH
15
16 to neutralize residual phosgene. In the glove box, the insoluble TEA·HCl was removed
17
18 by dissolving the product in 30% THF in hexanes and passing through a plug of vacuum
19
20 dried silica⁴⁹. The combined NCA containing fractions were dried under reduced
21
22 pressure and the product was dissolved in a minimal amount of THF and crystallized by
23
24 addition of hexanes (1:3 THF:hexanes). Multiple crystallizations (5x) were required for
25
26 adequate NCA purification (overall yield = 52%). ¹H NMR and FTIR spectral data were
27
28 consistent with previously reported values from literature⁵².

29 30 2.1.3. General Copolypeptide Synthetic Procedure

31
32 All polymerization reactions were performed in a N₂ filled glove box using anhydrous
33
34 solvents. To prepare copolypeptide at ca. 100 mg scale, a solution of Co(PMe₃)₄ (4.5
35
36 mg, 0.012 mmol) in THF (20 mg/mL) was quickly added to a solution of L-methionine
37
38 NCA (Met NCA; 100 mg, 0.57 mmol) and L-alanine NCA (Ala NCA; 7.3 mg, 0.063
39
40 mmol) in THF (50 mg/mL). To synthesize lysine containing copolypeptides, Ala NCA in
41
42 the above procedure was replaced with N-Boc-L-lysine NCA (Boc-Lys NCA) at the
43
44 desired molar ratio. After ca. 60 min., complete consumption of NCA was confirmed by
45
46 FTIR spectroscopy. In order to determine the lengths of poly(L-methionine-*stat*-L-
47
48 alanine), **MA**, or poly(L-methionine-*stat*-Boc-L-lysine), **MK^{Boc}**, segments, a small aliquot
49
50 (200 μl) of each polymerization mixture was removed for end-group analysis (*vide infra*).
51
52 To each remaining copolymerization mixture was then added L-leucine NCA (Leu NCA;
53
54 5.9 to 20 mg, 0.038 to 0.13 mmol) in THF (50 mg/mL). The Leu NCA monomers were
55
56 found to be completely consumed within ca. 60 min., and the reaction mixtures were
57
58 subsequently removed from the glove box. The block copolypeptide solutions were then
59
60 precipitated by addition to a 0.1 M aqueous HCl solution (75 mL), filtered, washed with
61
62 DI water, and dried under reduced pressure to yield white fluffy solids with yields
63
64
65

1
2
3
4 ranging from 90 to 95%. Detailed compositional and characterization data for all
5 samples are provided in the Supplementary Information.
6
7
8

9
10 *2.1.4. Sample procedure for **MA_m** chain length determination using end-group*
11 *analysis*
12

13 In the glove box, α -methoxy- ω -isocynoethyl-poly(ethylene glycol)₂₃ (mPEG₂₃-NCO)⁵³
14 (20 mg) was dissolved in THF (1 ml) in a 20 ml scintillation vial. An aliquot (200 μ l) of
15 copolymerization solution containing active chain ends (from 2.1.3 above) was removed
16 and added to the solution of mPEG₂₃-NCO. The PEG end-capped sample (e.g. **MA_m-**
17 **mPEG₂₃**) was sealed, allowed to stir for 24 h, and then used for chain length
18 determination. Outside of the glove box, the PEG end-capped sample was washed with
19 10 mM aqueous HCl (2x). After stirring for 1 h, **MA_m-mPEG₂₃** was collected by
20 centrifugation and washed with DI water (3 x 20 ml) to remove all non-conjugated
21 mPEG₂₃-NCO. The remaining **MA_m-mPEG₂₃** was then freeze-dried to remove residual
22 H₂O. To determine **MA_m** molecular weights (M_n), ¹H NMR spectra were obtained. Since
23 it has been shown that end-capping is quantitative for (PMe₃)₄Co initiated NCA
24 polymerizations when excess isocyanate is used⁵³, integrations of methionine (δ 2.70)
25 and alanine (δ 1.52) resonances versus the polyethylene glycol resonance at δ 3.92
26 could be used to obtain both the ratios of **M** to **A** and **MA_m** lengths.
27
28
29
30
31
32
33
34
35
36
37
38
39
40

41 *2.1.5. Procedure for Oxidation of Met Residues in Copolypeptides*
42

43 For Boc-Lys containing copolypeptides, deprotection was performed before oxidation of
44 Met residues (see 2.1.7). To convert Met residues in copolypeptides to Met sulfoxide
45 residues, a volume of 70 wt. % *tert*-butyl hydroperoxide (TBHP) (16 molar equivalents
46 per Met residue) was added to a sample of solid copolypeptide (ca. 80 mg). The
47 reaction mixture was then diluted with DI water to yield an overall polypeptide
48 concentration of ca. 20 mg/mL. To aid oxidation, a catalytic amount of camphorsulfonic
49 acid (CSA) (0.2 molar equivalents per Met residue) solution in DI water (20 mg/ml) was
50 subsequently added. The reaction mixture was stirred vigorously for 24 hours at
51 ambient temperature, whereupon complete dissolution of copolypeptide samples was
52 observed. Reaction mixtures were transferred to 2000 MWCO dialysis bags and
53
54
55
56
57
58
59
60
61
62
63
64
65

1
2
3
4 dialyzed against: (i) pyrogen free deionized milli-Q water (3.5L) containing sodium
5 thiosulfate (1.2 g, 2.16 mM) for 2 days to neutralize residual peroxide, (ii) milli-Q water
6 (3.5L) acidified to pH 4 with HCl for 2 days to aid cobalt ion removal, and (iii) milli-Q
7 water (3.5L) for 2 days to remove residual HCl. For each step dialysate was changed
8 every 12 hours. Copolyptide solutions were then freeze dried to yield white fluffy
9 solids with average yields of 90 to 95%, and 100% conversion of Met residues to Met
10 sulfoxide groups.
11
12
13
14
15
16
17
18

19 *2.1.6. Procedure for Methylation of Met Residues in Copolypeptides*

20 To convert Met residues in copolypeptides to S-methyl-Met sulfonium residues,
21 iodomethane (3 equivalents per Met residue) was added to suspensions of
22 copolypeptides (ca. 80 mg) in DI water (ca. 20 mg/ml). Reaction mixtures were covered
23 with aluminum foil to protect iodomethane from light, and then stirred vigorously for 5
24 days at ambient temperature. After 5 days, reaction mixtures were found to be
25 suspensions of particulates. The copolypeptides were subsequently transferred to 2000
26 MWCO dialysis bags and dialyzed against: (i) pyrogen free deionized milli-Q water
27 (3.5L) containing sodium metabisulfite (0.50 g, 0.75 mM) for 1 day to remove iodine
28 based impurities, (ii) milli-Q water (3.5L) acidified to pH 4 for 2 days to aid cobalt ion
29 removal, (iii) milli-Q water containing NaCl (7.0 g, 35 mM) for 2 days to facilitate iodide
30 to chloride counterion exchange, and (iv) milli-Q water (3.5L) for 2 days to remove
31 residual NaCl. For each step dialysate was changed every 12 hours. After dialysis all
32 copolypeptides were completely soluble in DI water. Copolypeptide solutions were then
33 freeze dried to yield white fluffy solids with average yields of 95 to 99%, and 99%
34 conversion of Met residues to S-methyl-Met sulfonium groups.
35
36
37
38
39
40
41
42
43
44
45
46
47
48
49

50 *2.1.7. Deprotection of Boc-Lys containing copolypeptides*

51 Deprotection of Boc-Lys was performed before oxidation of Met residues. To facilitate
52 deprotection, Boc-Lys containing copolypeptides (ca. 80 mg) were fully dissolved in
53 trifluoroacetic acid (ca. 25 mg/mL) and stirred at ambient temperature for 2 hours.
54 Copolypeptide samples were then precipitated into diethyl ether (75 mL). The diethyl
55
56
57
58
59
60
61
62
63
64
65

1
2
3
4 ether was decanted away and the copolypeptides were dried under reduced pressure
5 overnight to yield white solids (ca. 99% yield, 100% deprotection efficiency).
6
7
8

9 10 *2.1.8. Preparation of DCH Formulations*

11 DCH were prepared by solubilizing lyophilized copolypeptide in either DI water,
12 phosphate buffered saline (PBS), or cell culture media and allowing to assemble for 24
13 hours, without stirring, before use.
14
15
16
17

18 19 *2.1.9. Circular Dichroism*

20 All circular dichroism spectra were collected using an OLIS RSM CD spectrophotometer
21 (OLIS, USA) using conventional scanning mode. Poly(L-methionine sulfoxide), **M^O**, and
22 poly(L-methionine sulfoxide-*stat*-L-alanine), **M^OA**, samples were characterized by
23 recording spectra (185-260 nm) within a quartz cuvette of 0.1 cm path length. Samples
24 were prepared at concentrations of 0.10 to 0.17 mg/mL in Milli-Q water. The spectra
25 are reported in units of molar ellipticity $[\theta]$ ($\text{deg}\cdot\text{cm}^2\cdot\text{dmol}^{-1}$), which was calculated using
26 $[\theta] = (\theta \times 100 \times M_w)/(c \times l)$ where θ is the measured ellipticity (millidegrees), M_w is the
27 average residue molecular mass (g/mol), c is the polypeptide concentration (mg/mL),
28 and l is the cuvette path length (cm).
29
30
31
32
33
34
35
36
37
38

39 **2.2. DCH Characterization**

40 41 *2.2.1. Dynamic Mechanical Rheology*

42 Dynamic rheological measurements were performed at constant set temperature of 25
43 °C using a Physica MCR 301 (Anton Paar, Sweden) equipped with a 25 mm 1° cone
44 and plate geometry. To determine the linear viscoelastic testing region for each DCH
45 sample a frequency sweep from 0.1 to 100 rad s^{-1} at a fixed strain of 0.5% was applied
46 followed by a strain sweep from 0.1 to 100% strain at a fixed frequency of 10 rad s^{-1} .
47 DCH samples were allowed to recover for a period of 2 minutes between individual
48 rheological experiments. To compare mechanical properties across various DCH
49 samples a time sweep under fixed strain and frequency conditions (0.5% strain and 10
50 rad s^{-1}) was applied for one minute. To evaluate shear thinning and recovery behavior
51 of DCH the strain amplitude parameters were stepped from 0.5% to 1000%, maintained
52
53
54
55
56
57
58
59
60
61
62
63
64
65

1
2
3
4 at 1000% for 2 minutes and then returned to 0.5% to evaluate the recovery of the
5 mechanical properties at a fixed frequency of 10 rad s⁻¹.
6
7
8

9 10 **2.3. *In vitro* cell culture**

11 *2.3.1. Neural stem/progenitor cell (NSPC) derivation and culture*

12 Neural stem/progenitor cells (NSPC) used in this study were derived from mouse
13 embryonic stem cells (mESC). The mESC lines used in this study contain a Ribotag (a
14 modified ribosomal protein L22 (Rpl22) with hemagglutinin epitope tag)⁵⁴ allele. The
15 mESC lines were derived from the inner cell mass of E3.5 blastocyst stage embryos
16 generated from crosses of male homozygous B6N.129-Rpl22tm1.1Psam/J(StockNo:
17 011029) “Ribotag” mice to females hemizygous for a dominant, maternal effect cre
18 allele, B6.Cg-Tg(SOX2-cre)1Amc/J (StockNo: 008454) and heterozygous for the
19 “Ribotag” allele. Multiple male and female mESC lines were derived, and each was
20 karyotyped and genotyped to confirm sex and homozygosity for the cre-exised, Ribotag
21 allele. For generation of NSPC an induction and expansion method reported widely
22 within the literature was used⁵⁵⁻⁵⁷. Briefly, mESC were maintained and expanded on
23 gelatin-coated plates in DMEM media containing a cocktail of supporting growth factors
24 including Leukemia inhibitory factor (LIF) (EMD Millipore, Burlington, MA), ES grade
25 Fetal Bovine Serum (FBS), nucleosides, non-essential amino acids and β-
26 mercaptoethanol (Thermofisher Scientific). The neural induction of mESC was
27 performed using a 2-/4+ protocol described in detail previously⁵⁵. Specifically, 2X10⁶
28 mESC were cultured for two days in LIF free differentiation media (Advanced
29 DMEM/F12 media supplemented with knockout serum (Thermofisher Scientific),
30 glutamine, nucleosides, non-essential amino acids and β-mercaptoethanol) under non-
31 adherent suspension conditions to promote the formation of embryoid bodies (EB). After
32 two days the EBs were transferred to gelatin coated flasks and cultured for four days in
33 differentiation media supplemented with 50 nM retinoic acid (RA) and 500nM
34 purmorphamine (PUR)(sonic hedgehog (SHH) agonist) to caudalize and neurally induce
35 (NI) the cells⁵⁵. Differentiation media with the RA/PUR morphogens was replaced after
36 two days. Following neural induction the cells were subsequently expanded for several
37 passages in neural progenitor cell media (Advanced DMEM/F12 supplemented with
38
39
40
41
42
43
44
45
46
47
48
49
50
51
52
53
54
55
56
57
58
59
60
61
62
63
64
65

1
2
3
4 B27 (Thermofisher Scientific), nucleosides, non-essential amino acids, heparin and
5
6 FGF/EGF (Peprotech) both at 100 ng/ml) to generate a population of definitive NSPC
7
8 for *in vitro* studies. NSPC stocks that had undergone 15-24 passages (5-8 weeks of
9
10 neural expansion) were used for experimental studies.

11 12 13 *2.3.2. In vitro DCH NSPC viability evaluation*

14
15 To evaluate hydrogel cytotoxicity, NSPC were suspended within DCH formulations and
16
17 placed on top of 1% agarose molds containing unsupplemented Advanced DMEM/F12
18
19 media to ensure maintenance of hydrogel hydration. For each formulation 5000 cells/ μ L
20
21 of hydrogel were suspended within the material and 30 μ L of hydrogel/cell solution was
22
23 added on top of the agarose molds. Each hydrogel sample was studied in triplicate.
24
25 After 24 hours of incubation, hydrogels were thinned into liquids by dilution into 100 μ L
26
27 of 1X PBS containing 2 μ M Calcein AM to identify viable cells and 4 μ M EthD-1 to
28
29 identify dead cells and allowed to incubate at room temperature for 30 minutes. Cell
30
31 solutions were then transferred to glass slides, coverslipped and imaged using the FITC
32
33 and Rhodamine filters on an epi-fluorescent microscope (Zeiss). At least five images
34
35 per slide were collected resulting in a total of 15 images per hydrogel sample. Cell
36
37 viability was normalized to the viability of cells incubated in media alone.

38 39 *2.3.3. NSPC adhesion to DCH coated substrates*

40
41 Hydrophobic, siliconized circular glass coverslips (12mm) (Hampton Research, Aliso
42
43 Viejo, CA) or black 96 well untreated polystyrene plates (Brand, Germany) were coated
44
45 with an appropriate volume of 0.1 wt% copolypeptide solubilized in 70% ethanol. After
46
47 being allowed to adsorb for 1 hour, copolypeptide solutions were aspirated and the
48
49 coated surfaces allowed to dry for 1 hour under ambient conditions. Before plating the
50
51 cells, coated surfaces were washed once with water to remove any non-adsorbed
52
53 copolypeptide. Cells were seeded at 200,000 and 100,000 cells for the coverslips and
54
55 wells respectively and incubated on coated surfaces for 24 hours before analysis. For
56
57 the coated coverslips, the cells were imaged under brightfield conditions using an EVOS
58
59 XL cell imaging system (Thermofisher Scientific). After the 24 hour incubation period the
60
61 96 well plate was washed once with 1x PBS to remove non-adhered cells and the plate

1
2
3
4 was then treated with 1x PBS containing 2 μ M Calcein AM and 4 μ M EthD-1 for 30
5 minutes to identify viable cells that remained adhered to the plate. The 96 well plate was
6 read on a VICTOR 2V Multilabel fluorescent plate reader (Perkin Elmer). Quantification
7 of cell attachment was normalized to a gelatin coated substrate which demonstrated the
8 highest extent of cell adhesion.
9
10
11
12
13
14

15 2.3.4. NSPC differentiation on DCH substrates

16 To study the influence of cellular substrate interactions on NSPC differentiation
17 outcomes, 100 mm non-treated polystyrene petri dishes were coated separately with
18 DCH_{MO}, DCH_{MM} or gelatin. As in the adhesion experiments above, a 0.1 wt%
19 copolyptide solubilized in 70% ethanol was applied to each petri dish, allowed to
20 incubate and dry for 1 hour and then washed once with water to remove non-adsorbed
21 material. NSPC were seeded at a 2×10^6 cells/plate and cultured for 48 hours in media
22 containing 10% FBS. After 48 hours cells were trypsinized and re-seeded on gelatin
23 coated coverslips and cultured for an additional 72 hours in supplement free media to
24 promote spontaneous differentiation.
25
26
27
28
29
30
31
32
33
34

35 2.3.5. Immunocytochemistry

36 Cell seeded coverslips were washed with 1x PBS and fixed for 30 minutes with 4%
37 paraformaldehyde. Coverslips were then washed with TBS buffer, blocked and
38 permeabilized with donkey serum and Triton X-100 in TBS buffer before being stained
39 overnight with primary antibodies. Primary antibodies used within the *in vitro*
40 experiments included: (i) rat anti mouse-GFAP (ThermoFisher, #13-0300, 1:1000
41 dilution) (ii) rabbit anti mouse-TUJ-1 (Sigma, #T2200, 1:1000 dilution), (iii) goat anti-
42 mouse-HA (Novus, NB600-362, 1:1000 dilution), (iv) rabbit anti-mouse HA (Sigma,
43 H6908, 1:1000 dilution), (v) goat anti-mouse SOX2 (R&D Systems, AF2018, 1:300
44 dilution), (vi) goat anti-mouse SOX9 (Novus, H00006662-M02, 1:200 dilution) (vii)
45 chicken anti-mouse NESTIN (Novus, NB100-1604, 1:500 dilution). Fluorophore-
46 conjugated secondary donkey antibodies (Jackson ImmunoResearch) raised against
47 the various primary antibody species were applied for 2 hours. Coverslips were
48 subsequently stained for DAPI and mounted on glass slides.
49
50
51
52
53
54
55
56
57
58
59
60
61
62
63
64
65

1
2
3
4
5
6 2.3.6. *PCR*

7
8 NSPCs were seeded on DCH_{MO}, DCH_{MM} or gelatin coated 100 mm non-treated
9 polystyrene petri dishes at 6x10⁶ cells per plate and cultured in NSPC media containing
10 10% FBS. At 48 hours cells were lysed and mRNA isolated using the RNEasy® Plus
11 Mini RNA purification kit (Qiagen) following the manufacturer's instructions. Isolated
12 mRNA was quantified by UV/VIS and 500ng of mRNA was used to synthesize cDNA
13 using the iScript™ Reverse Transcription Supermix reagent (Biorad). qPCR was
14 performed as a 10 µL reaction volume in a 96 well PCR plate on a Lightcycler 96
15 instrument (Roche) and incorporating SsoAdvanced™ Universal SYBR® Green
16 Supermix (Biorad) and various primers (**Supplementary Table 1**). Relative gene
17 expression was determined by comparing Δct values for each experimental condition
18 that were normalized to the Ribotag (HA) gene expression.
19
20
21
22
23
24
25
26
27
28

29 **2.4. *In vivo* DCH injections**

30 2.4.1. *Surgery*

31
32 All surgical procedures used adhere to a protocol approved by the UCLA animal
33 research committee. Wildtype C57BL/6 mice (8-12 weeks) were used for all
34 experiments. For DCH injections, mice were anesthetized using isoflurane and a
35 craniotomy performed using a high speed surgical drill. A volume of 1 µL of DCH was
36 injected into the caudate putamen nucleus at 0.15 µL/min using target coordinates
37 relative to Bregma: +0.5 mm A/P, +2.5mm L/M and -3.0 mm D/V. DCH injections were
38 made using pulled glass micropipettes ground to a beveled tip with 150–250 µm inner
39 diameter attached via specialized connectors and high-pressure tubing to a 10 µL
40 syringe that was mounted to a stereotaxic frame and controlled by an automated
41 microdrive pump.
42
43
44
45
46
47
48
49
50
51

52 2.4.2. *Immunohistochemistry*

53
54 At 4 weeks after hydrogel injection mice underwent transcardial perfusion with
55 heparinized saline and 4% paraformaldehyde (PFA), and the brain was excised for
56 histological analysis. Following an 8 hour post fixation in 4% PFA and a 72hr incubation
57
58
59
60
61
62
63
64
65

1
2
3
4 in 30% sucrose, 40 µm coronal sections of brain were prepared using a cryostat. Tissue
5
6 sections were stained as free floating sections using standardized
7
8 immunohistochemistry techniques described by us elsewhere²⁶. Specific antibodies
9
10 used to stain brain tissue sections included: (i) rat anti mouse-GFAP (Thermofisher,
11
12 #13-0300, 1:1000 dilution) (ii) rabbit anti mouse-TUJ-1 (Sigma, #T2200, 1:1000
13
14 dilution), (iii) goat anti-mouse-HA (Novus, NB600-362, 1:1000 dilution), (iv) rabbit anti-
15
16 mouse HA (Sigma, H6908, 1:1000 dilution), (v) goat anti-mouse SOX2 (R&D Systems,
17
18 AF2018, 1:300 dilution), (vi) goat anti-mouse SOX9 (Novus, H00006662-M02,1:200
19
20 dilution), (vii) goat anti-mouse NESTIN (R&D Systems, AF2736, 1:800 dilution), (viii)
21
22 rabbit anti-mouse ALDH1L1 (Abcam, ab87117, 1:500), (ix) rabbit anti-mouse S100β
23
24 (Abcam, Ab41548, 1:1000), (x) rabbit anti-mouse NEUN (Abcam, AB177487, 1:800);
25
26 (xi) rabbit Neurofilament M (NFM) (EMD Millipore, AB1987, 1:1000). Fluorophore
27
28 conjugated secondary donkey antibodies (Jackson Immuno-Research) raised against
29
30 the various primary antibody species were applied for 2 hours. Tissue sections were
31
32 stained for DAPI before being mounted on glass slides and coverslipped with ProlongTM
33
34 Gold antifade mounting medium (Invitrogen).

3. Results

3.1. Synthesis of non-ionic and cationic Met-based DCH

3.1.1. Design and synthesis of Met-based DCH precursors

Using previous DCH as models, new copolypeptides were designed as amphiphilic diblock copolymers with conformationally disordered, hydrophilic modified poly(L-methionine), **M**, segments and α -helical hydrophobic poly(L-leucine), **L**, segments to promote hydrogel self-assembly in aqueous media. We initially planned to prepare precursor copolypeptides of the general structure poly(L-methionine)₁₇₀-*b*-poly(L-leucine)_{*n*}, **M**₁₇₀**L**_{*n*}, with *n* ranging from 15 to 40; where the **M** segments would then be oxidized or alkylated to give the DCH forming copolypeptides. However, an issue we observed when attempting to polymerize the long **M** segments required for DCH (> 150 residues) was that the resulting α -helical **M** chains strongly aggregate in the reaction solvent hindering the uniform addition of Leu NCA monomers for block copolymer preparation⁴⁹. Consequently, initial attempts to oxidize and alkylate Met residues in **M**₁₇₀**L**_{*n*} resulted in samples unable to form hydrogels (*vide infra*). In order to address the problem of α -helical **M** chain aggregation, we relied on previous observations that aggregation of hydrophobic helical polypeptides in organic solvents can be diminished by statistical addition of comonomers to disrupt side-chain packing^{24,49}. Hence, we incorporated small amounts of a non-ionic, low hydrophobicity comonomer, L-alanine (Ala), during **M** segment polymerization in order to disrupt packing of α -helical **M** chains and facilitate preparation of the desired diblock copolypeptide architectures⁵³.

Statistical copolymers of Ala NCA and Met NCA were prepared with target degrees of polymerization of *ca.* 100, where the Ala content was varied from 0 to 20 mol % (**Scheme 1**). The optimal Ala content was envisioned as the minimal amount required to disrupt polypeptide aggregation and allow efficient block copolypeptide synthesis. As expected, the **M**_{*m*} homopolymer containing no Ala formed an organogel in the reaction mixture due to chain aggregation. As the Ala content was increased, the poly(L-methionine-*stat*-L-alanine)_{*m*}, **MA**_{*m*}, copolymers became more soluble in the reaction mixture, and eventually resulted in free-flowing viscous liquids at compositions 10 mol%

1
2
3
4 Ala and above (**Scheme 1**). It is noteworthy that the incorporation of 10 mol% Ala did
5 not adversely affect the ability to obtain controlled NCA polymerizations required for
6 synthesis of well-defined block copolypeptides (**Supplementary Figure 1**). Also,
7 incorporation of 10 or 18 mol% Ala in **MA**_m copolymers was found to have only minimal
8 effect on the water solubility and disordered conformations of the corresponding
9 oxidized poly(L-methionine sulfoxide-*stat*-L-alanine)_m, **M^OA**_m, samples compared to **M^O**
10 homopolymer (**Supplementary Figure 2**)^{37,40}. Consequently, we selected **MA**
11 copolymer segments containing 10 mol% Ala as optimized compositions for use in Met-
12 based DCH.
13
14
15
16
17
18
19
20
21

22 Precursor diblock copolypeptides were then prepared containing **MA** segments ca. 170
23 residues long, followed by poly(L-leucine), **L**, segments of different length: poly(L-
24 methionine_{0.9}-*stat*-L-alanine_{0.1})₁₇₀-*b*-poly(L-leucine)_n, (**MA**)₁₇₀**L**_n, with *n* ranging from ca.
25 10 to 40 (**Scheme 2**). Previous studies on DCH showed that small variations of **L**
26 segment length have a much greater effect on DCH mechanical properties compared to
27 small variations in the hydrophilic segment length^{24,25}. All copolymers were isolated in
28 high yield with compositions that closely matched expected values (**Table 1**). The **MA**
29 segment length was chosen based on values known, from previous studies on
30 amphiphilic DCH²⁴, to be sufficiently long to promote hydrogel formation. The **L** lengths
31 were varied in order to study the role of hydrophobic composition on hydrogel formation
32 and properties. Oxidation or methylation of these precursors using established
33 methods^{33,40} was envisioned to yield the corresponding amphiphilic **M^O** derivatives (i.e.
34 DCH_{MO}) and **M^M** derivatives (i.e. DCH_{MM}), respectively, for evaluation as DCH (**Scheme**
35 **2**).
36
37
38
39
40
41
42
43
44
45
46
47
48
49

50 3.1.2. Synthesis of DCH_{MO} and DCH_{MM}

51 Complete and selective oxidation of (**MA**)₁₇₀**L**_n copolypeptides to the corresponding
52 sulfoxide derivatives, (**M^OA**)₁₇₀**L**_n (i.e. DCH_{MO}), was accomplished using *tert*-butyl
53 hydroperoxide (**Table 1, Supplementary Information NMR spectra**). We had
54 previously used hydrogen peroxide for this purpose with shorter Met containing
55 segments, but found that this reagent is not completely selective for MetO formation
56
57
58
59
60
61
62
63
64
65

1
2
3
4 when longer, less soluble Met containing copolymers are oxidized. Small amounts of
5 sulfone groups were observed to form with hydrogen peroxide (**Supplementary Figure**
6 **3**), which can adversely affect DCH_{MO} properties. As a different modification, selective
7 methylation of **(MA)₁₇₀L_n** copolypeptides to the corresponding S-methyl sulfonium
8 derivatives, **(M^MA)₁₇₀L_n** (i.e. DCH_{MM}), was accomplished using iodomethane, which gave
9 the modified copolypeptides in excellent yields (**Table 1, Supplementary Information**
10 **NMR spectra**). Both oxidation and methylation modifications of Met residues in these
11 copolypeptides result in conversion of the fully hydrophobic **(MA)₁₇₀L_n** precursors into
12 amphiphilic copolymers with potential to self-assemble in water and form DCH. Both
13 modifications also convert α -helical **MA** segments in the copolymers into
14 conformationally disordered **M^OA** and **M^MA** segments³⁰. The modifications differ in that
15 **M^OA** chains are non-ionic and hydrophilic, while **M^MA** chains are cationic and
16 hydrophilic.
17
18
19
20
21
22
23
24
25
26
27
28
29

30 3.1.3. Synthesis of DCH_{MOK}

31 To study how introduction of charged groups into DCH_{MO} affects hydrogel properties we
32 prepared a small series of samples where the Ala residues of DCH_{MO} were replaced
33 with L-lysine, Lys, residues. The Lys residues were expected to assist controlled
34 synthesis of long Met rich segments in a manner similar to Ala, as described above. In
35 addition, these residues, when protonated, will introduce cationic charges into the
36 hydrophilic segments of DCH_{MO}. Lys residues were introduced by copolymerization of
37 different fractions of N-*tert*-butoxycarbonyl-L-Lysine NCA (Boc-Lys NCA), with Met
38 NCA, followed by polymerization of the Leu block (**Supplementary Scheme 1**).
39 Deprotection of the Lys residues using TFA, followed by selective oxidation of the Met
40 residues gave the desired copolypeptides: poly(L-methionine sulfoxide_x-*stat*-L-lysine-
41 HCl_y)₁₇₀-*b*-poly(L-leucine)₂₃, **(M^O_xK_y)₁₇₀L₂₃**, with $x:y = 0.90:0.10$ (DCH_{MOK10}) and
42 0.85:0.15 (DCH_{MOK15}) (**Supplementary Scheme 1 and Supplementary Table 2**).
43 Copolymerization, subsequent deprotection and oxidation proceeded without issues,
44 showing that another comonomer beside Ala can be used to prepare well-defined
45 copolypeptides containing long Met rich segments. The introduction of charged Lys
46
47
48
49
50
51
52
53
54
55
56
57
58
59
60
61
62
63
64
65

1
2
3
4 residues into DCH_{MOK} was expected to affect both physical and biological properties of
5 these materials.
6
7

8 9 10 **3.2. Formulation and properties of Met-based DCH**

11 12 *3.2.1. Preparation and rheological properties of DCH_{MO} and DCH_{MM}*

13
14 For initial evaluation, all DCH_{MO} and DCH_{MM} samples, as well as Ala lacking (**M^O**)₁₇₀L₂₃
15 and (**M^M**)₁₇₀L₂₄ control samples, were separately mixed with deionized (DI) water at
16 concentrations ranging from 1.0 to 9.0 wt% (**Table 2**). These samples were briefly
17 agitated and then let stand for 24h, whereupon they were visually examined
18 (**Supplementary Figure 4**). At 1.0 wt%, all samples formed free-flowing, transparent
19 fluids. As concentrations were increased, all DCH_{MO} and DCH_{MM} samples were
20 observed to form hydrogels, except for those with the shortest L segments, (**M^OA**)₁₇₀L₁₂
21 and (**M^MA**)₁₇₀L₁₂, which were both transparent fluids up to 9.0 wt%. DCH_{MM} samples
22 were generally found to form hydrogels at lower concentrations compared to analogous
23 DCH_{MO} samples of similar composition. For all DCH_{MO} and DCH_{MM} samples with L₁₇
24 segments or longer, hydrogel formation improved with both L segment length and
25 sample concentration. However, in samples with longer L segment lengths and at
26 higher concentrations, copolyptide precipitation was also observed in these
27 hydrogels. Hydrogel opacity was generally more pronounced in the DCH_{MM} samples
28 relative to DCH_{MO} samples (**Supplementary Figure 4**). It is noteworthy that the Ala
29 lacking (**M^O**)₁₇₀L₂₃ and (**M^M**)₁₇₀L₂₄ samples were unable to form hydrogels
30 (**Supplementary Figure 5**), except for (**M^M**)₁₇₀L₂₄ that formed an opaque hydrogel at 9
31 wt%. These results confirm the importance of copolymerization of Ala residues into the
32 Met segments for DCH formation.
33
34
35
36
37
38
39
40
41
42
43
44
45
46
47
48
49

50
51 To quantify hydrogel properties, oscillatory rheology studies were conducted on select
52 DCH_{MO} and DCH_{MM} samples. For DCH_{MO} samples at 5.0 wt% in DI water, hydrogel
53 stiffness (G') was found to increase with L segment length up to L₂₈, yet precipitation in
54 samples with longer L segments reversed this trend (**Figure 1A**). Due to its desirable
55 combination of hydrogel stiffness and minimal turbidity, (**M^OA**)₁₇₀L₂₈ was chosen as an
56 optimized DCH_{MO} composition for further mechanical properties study. Preparation of
57
58
59
60
61
62
63
64
65

1
2
3
4 DCH_{MO} using different concentrations of (M^OA)₁₇₀L₂₈ in DI water was found to be a
5 convenient means to adjust hydrogel stiffness (**Figure 1B**). All samples formed clear
6 elastic hydrogels (G' » G'' over a range of frequency, **Figure 1C**), and their stiffness was
7 found to increase with higher copolyptide concentrations. The lack of visible
8 aggregates in these samples suggests that polymer chains were able to assemble into
9 the desired structures even at high concentrations. The self-healing properties of
10 DCH_{MO} after mechanical breakdown were studied by repeatedly subjecting a 5.0 wt%
11 (M^OA)₁₇₀L₂₈ sample in DI water to high amplitude oscillatory strain, and then monitoring
12 the recovery of elasticity over time by measuring G' at a much smaller strain amplitude
13 (**Figure 1D**). The periods of high strain resulted in G' dropping by two orders of
14 magnitude to below the level of G'', indicating the sample had become a viscous liquid.
15 Upon switching to low strain, the sample self-healed to recover its elastic properties,
16 with most of the original gel stiffness regained within the brief period (ca. 10 s) needed
17 to switch between strain amplitudes.
18
19
20
21
22
23
24
25
26
27
28
29
30

31
32 For DCH_{MM} samples at 5.0 wt% in DI water, hydrogel stiffness (G') was also found to
33 increase with L segment length up to L₃₃, and then leveled off as sample precipitation
34 occurred with longer L segments (**Figure 2A**). The increased hydrophilicity of the
35 charged M^M segments compared to non-ionic M^O segments may be responsible for the
36 significantly greater stiffness of these samples compared to DCH_{MO}. For reasons similar
37 to those stated for DCH_{MO}, (M^MA)₁₇₀L₂₇ was chosen as an optimized DCH_{MM}
38 composition for further mechanical properties study. Preparation of this DCH_{MM} at
39 different concentrations in DI water was similarly found to conveniently adjust hydrogel
40 stiffness (**Figure 2B**). All samples formed elastic hydrogels (G' » G'' over a range of
41 frequency, **Figure 2C**) with stiffness that increased with higher copolyptide
42 concentrations. However, in contrast to DCH_{MO} of similar composition, visible
43 aggregates were observed at sample concentrations greater than 5.0 wt%. The 5.0 wt%
44 (M^MA)₁₇₀L₂₇ sample in DI water was also able to exhibit shear thinning and self-healing
45 properties comparable to results observed above with DCH_{MO} (**Figure 2D**).
46
47
48
49
50
51
52
53
54
55
56
57
58

59 3.2.2. Effects of ionic media on DCH_{MO} and DCH_{MM}

60
61
62
63
64
65

1
2
3
4 Select DCH_{MO} and DCH_{MM} samples ((M^OA)₁₇₀L₂₄ and (M^MA)₁₇₀L₂₃) were also prepared
5
6 in different aqueous media (**Figure 3**). We used these samples, containing L_{23/24}
7
8 hydrophobic segments, since their mechanical properties were closest to those of
9
10 hydrogel formulations we have found to be useful for CNS applications. Samples were
11
12 prepared at 5 wt% in either DI water, 1x PBS buffer, or DMEM cell culture medium, and
13
14 their rheological behavior studied. Mechanical properties of the non-ionic DCH_{MO}
15
16 formulations were minimally affected by the ions present in media (**Figure 3A, B**),
17
18 allowing for predictable mechanical behavior under different solution conditions.
19
20 Conversely, mechanical properties of the cationic DCH_{MM} formulations were strongly
21
22 affected by the ions present in media (**Figure 3C,D**), with hydrogel stiffness (G')
23
24 decreasing significantly in the presence of ions compared to DI water. Notably, different
25
26 media (PBS and DMEM) had similar effects on DCH_{MM} properties, and the DCH_{MM} in
27
28 these media remained hydrogels with stiffness comparable to analogous DCH_{MO}
29
30 formulations. Another difference observed between DCH_{MO} and DCH_{MM} formulations
31
32 was their breakdown at elevated percent strain. The DCH_{MM} formulations were found to
33
34 be more brittle than analogous DCH_{MO} formulations, especially in ionic media, where
35
36 the DCH_{MM} samples were observed to breakdown at relatively low percent strain
37
38 (**Figure 3B, D**). As shown above, at very high percent strains (ca. > 1000%), both
39
40 DCH_{MO} and DCH_{MM} will break down into liquids.

3.2.3. Rheological properties of DCH_{MOK}

41
42 The Lys containing samples DCH_{MOK10} and DCH_{MOK15} were mixed with DI water
43
44 or 1x PBS to give concentrations of 5.0 wt% and were found to form hydrogels in both
45
46 media after standing for 24h. In DI water, DCH_{MOK10} and DCH_{MOK15} formed hydrogels
47
48 with stiffness (G') intermediate between those of DCH_{MO} and DCH_{MM} at similar
49
50 compositions (**Figure 4, Supplementary Figure 6**). Hydrogel stiffness was found to
51
52 increase with increased ionic residue content in the DCH, where even 15 mol% charged
53
54 residues in the hydrophilic DCH segments was sufficient to result in hydrogel stiffness
55
56 comparable to that obtained with the fully charged segments in DCH_{MM}. Increased
57
58 charged residue content also significantly impacted hydrogel salt stability, where
59
60 DCH_{MOK15} was found to weaken significantly in PBS, similar to DCH_{MM}. DCH_{MOK10}
61
62
63
64
65

1
2
3
4 behaved more like DCH_{MO} in PBS, where hydrogel stiffness was even found to increase
5
6 in ionic media. From these observations, it can be seen that small variations in charged
7
8 residue content in DCH_{MOK} can result in substantial effects on both hydrogel stiffness
9
10 and salt stability.

11 12 13 **3.3. NSPC viability in Met-based DCH**

14
15 For CNS cell transplantation a cell compatible biomaterial vehicle that promotes
16
17 negligible cytotoxicity is required. To test the cell viability of Met-based DCH materials
18
19 we derived a passagable, adherent neural stem/progenitor cell (NSPC) line from mouse
20
21 embryonic stem cells (ESC) using previously validated and published protocols
22
23 **(Supplementary Figure 7A)**⁵⁵⁻⁵⁷. The use of an ESC derived NSPC line overcame
24
25 many of the quality and reproducibility limitations associated with using primary cells
26
27 harvested from fetal or post-natal tissue that we have employed in our previous
28
29 studies^{28,53}. Before encapsulating cells in DCH formulations we confirmed NSPC
30
31 derivation by qPCR and immunohistochemical analysis **(Supplementary Figure 7B)**.
32
33 The adherent NSPC line showed characteristic increased expression of canonical
34
35 neural stem cell genes (*Nestin, Sox2, Sox9, Olig2*) as well as a de-enrichment of classic
36
37 ES identifiers *Nanog* and *Oct4* **(Supplementary Figure 7B)**. Immunocytochemical
38
39 staining further confirmed robust protein expression of the same canonical neural stem
40
41 cell markers in our NSPC line **(Supplementary Figure 7C, D)**. The NSPC used in this
42
43 study contain a hemagglutinin (HA) tag on ribosomal protein L22, a component of the
44
45 60S ribosomal subunit (referred to here as Ribotag). This Ribotag can be used as an *in*
46
47 *vivo* reporter to distinguish transplanted NSPCs from host cells by
48
49 immunohistochemistry as well as allowing for cell specific translating mRNA extraction
50
51 from whole tissue⁵⁴. We confirmed 100% expression of the HA Ribotag in every cell in
52
53 the NSPC line by immunocytochemistry **(Supplementary Figure 7E)**. The NSPC line
54
55 showed negligible expression of the pan astrocyte marker GFAP and pan neuronal
56
57 marker TUJ-1 by immunohistochemical staining under regular culture conditions.
58
59 However, NSPC showed a competency to differentiate into these two cell types upon
60
61 exposure to fetal bovine serum (FBS) enriched media consistent with previous
62
63 characterization of similar NSPC lines **(Supplementary Figure 7E₁)**^{56,58}. Before and
64
65

1
2
3
4 after neuronal or astrocyte differentiation the cells maintained robust HA expression that
5 filled the entire cell cytoplasm (**Supplementary Figure 7E₂**).

6
7
8
9
10 To evaluate the relative cell compatibility of the various Met-based DCH vehicles we
11 encapsulated NSPC within DCH_{MO}, DCH_{MM}, DCH_{MOK10} and DCH_{MOK15} formulations and
12 incubated the cell-hydrogel construct on top of beds of cell media enriched agarose gels
13 for 24 hours. Specific copolyptide compositions used in these and all subsequent
14 biological studies were (M⁰A)₁₇₀L₂₄, (M^MA)₁₇₀L₂₃, (M⁰_{0.90}K_{0.10})₁₇₀L₂₃, and (M⁰_{0.85}K_{0.15})₁₇₀L₂₃.
15 Cell viability was determined by analyzing the distribution of live and dead cells using
16 calcein AM and ethidium homodimer-1 staining. The non-ionic DCH_{MO} showed excellent
17 NSPC viability for all formulations tested from 2 to 5 wt% copolyptide. The negligible
18 cytotoxicity for DCH_{MO} over the 24 hour period was equivalent to that observed for the
19 positive control of cells alone in media (**Figure 5A, B, D**). By contrast DCH_{MM}
20 formulations containing positively charged sulfonium functional groups demonstrated
21 substantial NSPC cytotoxicity which was equivalent to the cell death observed for
22 DCH_K, another cationic copolyptide hydrogel we have shown previously to be
23 cytotoxic towards various suspended cells^{28,53} (**Figure 5A, D**). The Lys containing
24 hydrogels DCH_{MOK10} and DCH_{MOK15} showed reduced NSPC viability compared to
25 DCH_{MO} with cytotoxicity increasing in a Lys concentration dependent manner.
26 Specifically, DCH_{MOK10} showed 80.7% NSPC viability while DCH_{MOK15} demonstrated
27 comparable cytotoxicity to that observed for DCH_{MM} and DCH_K suggesting this to be the
28 minimum Lys content required within DCH polypeptides for complete lysis of suspended
29 cells. (**Figure 5C**).

3.4. NSPC adhesion to Met-based DCH

40
41
42
43
44
45
46
47
48 Cell-biomaterial interactions may influence NSPC transplant outcomes⁵⁹. Since M⁰
49 polypeptides have previously been demonstrated to be non-fouling, bioinert substrates
50 for cells *in vitro*⁴¹, we sought to evaluate NSPC interactions with Met-based DCH. To
51 achieve this, we assessed the ability of NSPC to adhere to substrates coated with the
52 various Met-based DCH and compared and normalized them to a standard cell
53 adhesion promoting biomolecule, gelatin, which is used widely across adherent *in vitro*
54
55
56
57
58
59
60
61
62
63
64
65

1
2
3
4 assays. The use of 70% ethanol solutions of Met-based DCH ensured robust
5 copolypeptide coating to either hydrophobic siliconized glass slides or hydrophobic
6 untreated polystyrene. Calcein AM staining after vigorous washing to remove non-
7 adhered cells was used to quantify the amount of viable adhered cells to each
8 substrate. At 24 hours after seeding NSPC in FBS enriched media, DCH_{MO} showed
9 negligible NSPC adhesion (0.23% of the gelatin coated substrate cell number) and
10 instead led to significant cell aggregation resulting in large clumps of cells that were
11 hundreds of μm in diameter (**Figure 6A, B, Supplementary Figure 8**). The minimal cell
12 adhesion was equivalent to that achieved for the amphiphilic PEG based negative
13 control. By contrast, the DCH_{MM} with 63.2% adhered cells was comparable to that seen
14 for the positively charged Lys based DCH_K (74.3%) with cells displaying a characteristic
15 adherent, flattened morphology by brightfield microscopy (**Figure 6A, B**). Introduction of
16 cationic charge within DCH_{MO} via replacement of Ala with Lys residues (i.e. DCH_{MOK10},
17 DCH_{MOK15}) increased the cellular interactions with the copolypeptide chains and
18 consequently increased cell adhesion to coated substrates. Cell adhesion increased in
19 a Lys concentration dependent manner with DCH_{MOK10} maintaining 30.3% cell adhesion
20 while DCH_{MOK15} showing 76.7% cell adhesion. Cells on surfaces of DCH_{MOK10} adhered
21 as small multi-cellular aggregates that were smaller in size than those seen in the
22 DCH_{MO} samples with some flattened adherent cells visible at the margins of the
23 aggregate (**Figure 6B**). The extent of cell adhesion for DCH_{MOK15} was comparable to
24 DCH_K and DCH_{MM} suggesting that the charge distribution on the DCH_{MOK15} represented
25 the minimum amount of net charge needed along DCH copolypeptide chains to promote
26 significant interaction with NSPC. Interestingly, the cell adhesion data was inversely
27 related to the observed cell viability results articulated above when NSPC were
28 suspended within the same DCH formulation. These data suggest that non-specific
29 cationic charge based cell interactions can robustly encourage NSPC to adhere to a
30 constrained two dimensional substrate with negligible cytotoxicity. However, when the
31 cells are immersed within DCH containing the same hydrophilic chains, the strength and
32 concentration of these polymer-cell interactions, which are less constrained in space
33 and undergo dynamic movement around the encapsulated NSPC, results in cell
34 membrane disruption and/or lysis causing cell death.

3.5. NSPC differentiation with Met Based DCH

Physical interactions of stem cells with the extracellular matrix environment are principal determinants of cell fate decision making⁶⁰. Similarly, NSPC differentiation outcomes upon transplantation in the CNS are also influenced by their interactions with biomaterial carriers⁶¹, as well as with host tissue elements. To understand how cellular interactions with the Met-based DCH influence NSPC cell fate outcomes we devised an assay to evaluate NSPC differentiation on DCH coated substrates. Towards replicating the environment the transplanted NSPC would experience *in vivo* within the context of CNS injury we cultured NSPC in media containing 10% FBS along with standard NSPC supplements (EGF, FGF and B27). NSPC differentiation was evaluated on substrates of DCH_{MO}, DCH_{MM} or gelatin for 48 hours. After 48 hours in this serum rich environment the cells were transferred to unsupplemented conditions on gelatin substrates to evaluate the spontaneous differentiation of these cells following FBS treatment (**Figure 7A**). NSPC differentiation was significantly influenced by the chemical properties of the substrate (**Figure 7B, C, Supplementary Figure 9**). NSPC cultured on gelatin during the 48 hours of FBS exposure exhibited a significantly increased density of GFAP positive cells normalized to HA positive cell signal (a measure of total surface area occupied by cells on the substrate) compared to the DCH_{MO} and DCH_{MM} coated substrates. By contrast, a predominately neuronal differentiation phenotype (as measured by TUJ-1 positive cell density) was observed on the DCH_{MM} coated substrate. The DCH_{MO} coated surface, unlike the two cell adhesive substrates, exhibited no clear dominant differentiated cell type and showed an overall reduced extent of total cell differentiation that was approximately half of that observed on the gelatin surface (**Figure 7C**). To understand why the DCH_{MM} coated substrate showed a preferred neuronal differentiation profile compared to gelatin, we compared NSPC phenotypes immediately after FBS exposure by immunocytochemistry (**Figure 7D**). While gelatin coated substrates showed a dense field of GFAP and TUJ-1 positive cells at the conclusion of FBS treatment, cells on DCH_{MM} expressed exclusively TUJ-1 that was distributed diffusely throughout the cell cytoplasm rather than being organized in ordered, filamentous cytoskeletal structures that is characteristic of cultured neurons.

1
2
3
4 NSPC cultured on DCH_{MM} were also less dense in number and exhibited a larger and
5
6 more flattened cell morphology with extensive filopodia projections that varied in shape
7
8 and size between different cells throughout the surface. The relative strength of the cell
9
10 interactions with the DCH_{MM} substrate was further characterized by assessing the
11
12 number of cells that remained on the surface following a trypsinization procedure
13
14 **(Figure 7E)**. While complete cell removal off of the gelatin surface was achieved
15
16 following trypsinization, approximately 12% viable cells remained on DCH_{MM} following
17
18 the same procedure. This residual adhered cell number is likely an under estimate of
19
20 the total remaining cells after trypsinization as this procedure can be considerably
21
22 cytotoxic to persistently adhered cells and our outcome measure (Calcien AM staining)
23
24 only identified live, viable cells. Regardless of the exact percentage of remaining cells,
25
26 the relatively high number of residual cells comparatively to the gelatin substrate
27
28 coupled with the flattened, irregular cell morphology suggests a particularly strong cell
29
30 interaction with DCH_{MM}. Additionally, qPCR was performed on cells collected at the end
31
32 of the 48 hour FBS treatment to evaluate the effect of surface properties on the gene
33
34 expression of neural stem cell and neural cell type specific markers **(Figure 7F)**. In line
35
36 with the immunocytochemistry data, cells cultured on DCH_{MO} showed a more preserved
37
38 progenitor-like gene profile upon FBS exposure with canonical neural stem cell genes
39
40 *Nestin* and *Sox9* being less down regulated in this group compared to cells cultured on
41
42 the adhesive substrates. Interestingly, *GFAP* gene expression was highest for DCH_{MO}
43
44 over all other groups, while *GFAP* was also significantly expressed by cells on DCH_{MM}.
45
46 The mismatch between *GFAP* mRNA abundance and protein expression levels
47
48 measured by immunocytochemistry across the different treatments suggests that the
49
50 physical substrate and how cells interact with it may influence important cellular
51
52 functions such as mRNA post transcriptional modifications, protein synthesis and
53
54 cytoskeletal protein assembly. Overall, these data suggest that the non-adhesive
55
56 DCH_{MO} preserves the multipotency of NSPC in serum rich environments compared to
57
58 adhesive materials. This unique biological property of DCH_{MO} may prove to be useful for
59
60 ensuring robust survival and integration of transplanted NSPC within CNS injury
61
62 microenvironments.
63
64
65

3.6. *In vivo* NSPC transplantation using Met-based DCH

To evaluate the utility of Met-based DCH as biomaterial carriers for CNS transplantation we first injected empty DCH_{MO} into the uninjured mouse striatum and compared the induced foreign body response to a saline control. DCH_{MO} alone caused minimal host CNS tissue disruption. Specifically, the proximal neuronal survival as well as the extent and magnitude of the reactive astroglial response for the DCH_{MO} was comparable to that of the saline injection (**Supplementary Figure 10**). Next, we transplanted NSPC encapsulated within DCH_{MO} into the uninjured mouse striatum. The NSPC suspended uniformly within DCH_{MO} and did not sediment or aggregate throughout the entire duration of both the glass pipette loading and the slow controlled injection procedure, which was similar to that seen for our previously studied formulations²⁸. Gene profiling of NSPC suspended within DCH_{MO} recovered from the un-injected fraction of biomaterial at 6 hours after initial cell loading showed negligible change in gene expression of canonical neural stem cell genes for the injected cells compared to the *in vitro* cultured NSPC line (**Supplementary Figure 11**). At 4 weeks after transplantation NSPC injected brains were analyzed by immunohistochemistry (**Figure 8**). Injected NSPC loaded in DCH_{MO} formed an obvious and focal deposit within host tissue that persisted over the 4 week observation period. Transplanted cells as well as any potential progeny were readily identified by HA immunohistochemical staining. Transplanted cells were observed within the hydrogel as multicellular neurosphere aggregates that had adhered to the margins of the hydrogel deposit and subsequently integrated with host tissue (**Figure 8**). Within host tissue, transplanted cells were constrained within a tissue volume region that was within several hundred μm of the border of the hydrogel deposit (**Figure 8**). Thus the use of the DCH_{MO} vehicle prevented long distance migration of transplanted cells away from the injection zone to other brain regions. Essentially all transplanted cells expressed GFAP robustly by 4 weeks but also maintained widespread expression of the canonical neural stem cell markers SOX9 (**Figure 8A, B**), SOX2 (**Figure 8C**) and NESTIN (**Figure 8D**) characteristic of an immature astroglial phenotype⁵⁸. This extensive GFAP expression represented an upregulation of this astroglial marker compared with the NSPC at the time of transplantation. Grafted cells were uniformly negative for the neuronal marker TUJ-1

1
2
3
4 (Supplementary Figure 12). By four weeks the numerous transplanted cells that had
5 integrated into the adjacent host tissue had adopted distinct, individual cellular domains
6 reminiscent of normal host astroglial cells⁶² (Figure 8B).
7
8
9

10
11 Immunohistochemical evaluation revealed that host neurons (Figure 9) and host
12 astrocytes (Figure 10) persisted with normal density and viability at the edge of the
13 NSPC graft margin. HA positive transplanted cells with their GFAP positive cellular
14 processes integrated into fields of, and interacted directly with, host NEUN positive
15 neurons (Figure 9A, B). In addition to direct interactions with neuronal somas, grafted
16 cells showed a capacity to act as cellular substrates to attract and support the growth of
17 host axons. Specifically, using Neurofilament M (NFM) to label host axons, we observed
18 that the transplanted NSPC functioned as cellular bridges permitting regrowth of
19 meandering host axons into the DCH_{MO} deposit site (Figure 9C, D). Such a function is
20 consistent with the role host immature astroglia play during CNS development to
21 support and guide axon growth⁶³ and may be important for promoting regeneration of
22 damaged axons in the context of CNS injury^{26,28,64}. While the HA positive transplanted
23 cells expressed high levels of GFAP, they did not express the more mature astrocyte
24 marker ALDH1L1 (Figure 10A, C), further supporting the notion that these cells had
25 persisted as immature astroglial cells throughout the 4 weeks of residence in the
26 uninjured CNS^{56,65}. Some HA positive cells expressed an alternative but less mature
27 astrocyte marker, S100 β , suggesting the transplanted cells may be progressing through
28 astrocyte maturation. However, S100 β expression was not widespread among all
29 transplanted cells (Figure 10B). Despite their immature phenotype, grafted cells were
30 observed to interact directly, and intermingle, with host astrocytes (Figure 10C). Host
31 astrocytes were also observed to migrate into the persistent DCH_{MO} deposit site that
32 contained a high density of grafted cells (Figure 10A, B), creating a fluid transition of
33 intermingled host and grafted astroglia at the margins of the graft deposit. Furthermore,
34 at the margins of the DCH_{MO} deposit there was no evidence of host astrocyte scarring
35 or walling off of the NSPC-hydrogel implant, while host astrocytes in close proximity of
36 the DCH deposit margin were only mildly reactive and maintained discrete individual
37 cellular domains. Overall, these findings suggest that NSPC transplanted in DCH_{MO} can
38
39
40
41
42
43
44
45
46
47
48
49
50
51
52
53
54
55
56
57
58
59
60
61
62
63
64
65

1
2
3
4 provide cells that integrate well with receptive host neural tissue and serve supportive
5 functions that may be useful for neural repair.
6
7
8

9 10 **4. Discussion**

11 In this study, we developed a novel biomaterial platform focused on the post-
12 polymerization modification of Met-based copolypeptides. These new materials show
13 diverse and tunable physiochemical and biological properties with some formulations
14 demonstrating utility as vehicles for aiding the *in vivo* transplantation of NSPC in the
15 CNS. Our findings have implications at several levels, including (i) the technical
16 development of non-ionic biomaterial vehicles for NSPC delivery; (ii) the influence of
17 Met-based DCH on NSPC survival and differentiation; and (iii) the potential of Met-
18 based DCH for NSPC transplantation into injured CNS.
19
20
21
22
23
24
25
26
27

28 **4.1. Technical considerations regarding development of non-ionic, Met-based** 29 **DCH** 30

31 We have shown previously that ionic DCH such as DCH_K are useful vehicles for delivery
32 of both small molecule and protein biologically active agents into mouse CNS tissues *in*
33 *vivo*. In particular, the modular design of DCH permits fine tuning of their physical
34 characteristics for specific applications, and their synthetic nature allows for scalable
35 synthesis and reproducible formulation. An initial effort to prepare non-ionic DCH for
36 encapsulation of cells *in vitro* and their grafting into tissues *in vivo* used synthetic
37 methods relying on unnatural amino acid components that limited scalability and
38 prohibited incorporation of functionality into these DCH²⁸. To correct these limitations,
39 we envisioned Met-based DCH as a versatile platform of precursor copolypeptides that
40 could be selectively modified at Met residues using a variety of efficient procedures to
41 give DCH with different physical and biological properties. Initial targets for evaluation
42 were non-ionic DCH_{MO} and a model cationic derivative, DCH_{MM}.
43
44
45
46
47
48
49
50
51
52
53

54
55
56 Aggregation of **M** polymers during synthesis was an initial hurdle that was overcome by
57 judicious addition of comonomers, i.e. Ala and Lys, which were found to disrupt helical
58 side-chain packing of **M** segments and thus enabling controlled synthesis of Met DCH
59
60
61

1
2
3
4 precursors. The need to incorporate comonomers in the **M** segments was found to be
5 advantageous, as they can provide additional means to fine tune DCH properties. Ala
6 residues were found to act as inert diluents that imparted no adverse effects on the
7 properties of the modified **M** segments. Incorporation of Lys residues was found to be a
8 useful means to introduce controllable quantities of charged residues into **M^O** segments.
9 Another potentially useful feature of these Met DCH precursors is that some of the Met
10 or Lys residues can also serve as sites for selective conjugation of bioactive molecules
11 or fluorescent probes for added functionality³⁰.
12
13
14
15
16
17
18
19
20

21 Straightforward modification of Met DCH precursors using literature methods gave non-
22 ionic DCH_{MO} and cationic DCH_{MM} with near quantitative levels of functionalization in
23 excellent yields. Both DCH_{MO} and DCH_{MM} of different compositions formed hydrogels
24 over a range of concentrations in DI water. At equivalent compositions and
25 concentrations, DCH_{MO} formed inherently weaker hydrogels compared to DCH_{MM}, which
26 is likely due to the greater water solubility, and electrostatic repulsions in the cationic
27 **M^MA** segments compared to non-ionic **M^OA** segments. However, DCH_{MO} were found to
28 be more ductile and stable to ionic media compared to DCH_{MM}, such that hydrogel
29 stiffness of comparable samples was very similar in ionic media. This finding is
30 important since both of these hydrogels will be used primarily in ionic media for all
31 biological studies. Overall, both DCH_{MO} and DCH_{MM} were found to possess desirable
32 physical properties for evaluation as vehicles in CNS applications, including injectability
33 and tunable stiffness and surface functionality. We were particularly interested to study
34 how variation of charge content in DCH_{MO}, DCH_{MOK} and DCH_{MM} affects how these
35 hydrogels interact with cells.
36
37
38
39
40
41
42
43
44
45
46
47
48
49

50 **4.2. The influence of Met-based DCH on NSPC survival and differentiation**

51 Cues from the extracellular environment both within *in vitro* culture conditions and
52 neural tissue niches *in vivo* shape the differentiation decision making of NSPC. Detailed
53 experimental information pertaining to the relative importance of various stimuli,
54 including the physiochemical properties of biomaterial carriers, on NSPC differentiation
55 is beginning to emerge²². In particular, properties such as mechanical stiffness and
56
57
58
59
60
61
62
63
64
65

1
2
3
4 biomaterial degradability have been extensively studied⁶³. Here, by leveraging the
5 physiochemical tunability of Met-based DCH through various post-polymerization
6 modifications, we characterized and optimized the effect of biomaterial surface
7 chemistry on NSPC differentiation. DCH_{MO} by virtue of its non-fouling sulfoxide
8 functionality showed a remarkable preservation of neural stemness in a serum rich *in*
9 *vitro* environment compared to adhesive substrates DCH_{MM} and Gelatin. To improve
10 survival of NSPC upon transplantation in traumatic CNS lesions a biomaterial carrier
11 capable of keeping the cells in a more robust immature state for longer upon grafting
12 would be advantageous.
13
14
15
16
17
18
19
20
21

22 In addition to the development of a novel hydrogel we also describe here for the first
23 time the derivation of a Ribotag NSPC line. Ribotag is a cell specific mRNA isolation
24 technique from whole tissue that has gained in popularity over the past several
25 years^{26,54,66}. This paper describes and validates the derivation of the Ribotag NSPC line
26 from transgenic ESC and demonstrates the preservation of detectable HA positive
27 ribosomes within cells throughout the various stages of NSPC development and
28 differentiation. While not explored here, the goal for the use of these cells in future
29 experiments is to perform *in vivo* transplant cell specific genetic evaluation in the
30 context of CNS injury. This paper represents a first step towards this goal by
31 demonstrating the ability to: (i) detect HA positive NSPC and their progeny by
32 immunohistochemistry *in vitro* and in whole tissue after grafting *in vivo*, as well as (ii)
33 characterize the robustness of Ribotag mRNA expression within cells at various stages
34 of development both *in vitro* and *in vivo* such that it could be used as a housekeeping
35 gene to normalize gene expression data. Furthermore, the robust and persistent
36 expression of Ribotag by NSPC and their progeny *in vivo*, provides a means of selective
37 isolation of transcribed mRNA specifically from grafted cells for analysis of changes in
38 their transcriptional profiles at different times after transplantation and under different
39 grafting conditions. Given the interesting findings pertaining to the variation in NSPC
40 differentiation *in vitro* as a function of material surface properties and exposure to
41 different morphogens, future experiments using these cells can be directed towards
42
43
44
45
46
47
48
49
50
51
52
53
54
55
56
57
58
59
60
61
62
63
64
65

1
2
3
4 obtaining a detailed understanding of the effect of hydrogel carrier properties and
5 effects of co-delivery of regulatory molecules on NSPC differentiation *in vivo*.
6
7
8

9 10 **4.3. The potential of Met-based DCH for NSPC transplantation into CNS injury**

11 In the context of CNS insults such as spinal cord injury, traumatic brain injury or stroke
12 damage of neural tissue results in a biologically conserved wound healing response that
13 leads to the formation of non-neural tissue (NNT) lesions^{67,68}. NNT lesions hinder
14 endogenous recovery/regeneration of damaged neural circuitry as this tissue is
15 permanently devoid of functioning neurons and glia. Grafting of NSPC has emerged as
16 a potential therapy for CNS injury by repopulating NNT lesions with a neural cell milieu
17 that can provide both the trophic support and physical substrates necessary to aid the
18 axon regeneration required to reestablish functioning circuits⁶⁸. In this study we showed
19 that transplanted NSPC, in the absence of differentiation directing morphogens, adopt
20 immature astroglial phenotypes at 4 weeks that were capable of interacting with host
21 astrocytes and neurons as well as acting as a cellular substrate for regrowing axons
22 locally in the vicinity of the injected hydrogel. DCH_{MO} aided in keeping transplanted cells
23 local to the injection site but still permitted comprehensive integration with host neural
24 tissue. Transplanted cells adopted an immature astroglial cell state (as demonstrated by
25 robust GFAP, SOX2, SOX9 and NESTIN expression) and no transplanted cells
26 expressed the pan-neuronal marker TUJ-1 or the mature astrocyte marker ALDH1L1.
27 These results indicate that, in the absence of co-delivery of differentiation directing
28 morphogens, these cells do not undergo any significant spontaneous differentiation and
29 maturation *in vivo*, at least up to 4 weeks. We have previously shown that DCH vehicles
30 can be used to controllably delivery a variety of small molecule and protein based drugs
31 to the CNS²⁶. Therefore, future studies will explore using DCH_{MO} to co-deliver both
32 NSPC and specific bioactive morphogens to facilitate specific *in vivo* directed
33 differentiation and maturation of transplanted cells.
34
35
36
37
38
39
40
41
42
43
44
45
46
47
48
49
50
51
52
53
54
55

56 **5. Conclusion**

57 In this study we developed a new Met-based DCH platform that overcame several
58 synthetic limitations associated with previous formulations and demonstrated tunable
59
60
61
62
63
64
65

1
2
3
4 physiochemical and biological properties. Met-based DCH also offer considerable
5 flexibility in terms of converting Met residues to different functional derivatives, as well
6 as the ability to incorporate different amino acid comonomers into their hydrophilic
7 segments. The non-ionic DCH_{MO} formulations were found to be advantageous for cell
8 transplantation applications since they possess: (i) favorable cytocompatibility, (ii) cell
9 non-fouling properties, and (iii) an ability to better persevere NSPC stemness in serum
10 rich environments compared to adhesive substrates. DCH_{MO} facilitated local injection
11 and retention of NSPC and its progeny in the uninjured mouse CNS. In the absence of
12 added morphogens, transplanted cells maintained an immature astroglial phenotype at
13 4 weeks that favorably interacted with host neural tissue and acted as a cellular
14 substrate to aid regeneration of host-derived damaged or sprouted axons. These
15 findings suggest that DCH_{MO} is a suitable hydrogel carrier for neural stem cell
16 transplantation applications and warrants further investigation as a therapeutic tool in
17 CNS injury studies.
18
19
20
21
22
23
24
25
26
27
28
29
30
31
32

33 **Acknowledgements**

34 We thank the Microscopy Core Resource of the UCLA Broad Stem Cell Research
35 Center-CIRM Laboratory as well as the lab of Tatiana Segura at UCLA for generously
36 providing access to equipment for the rheological experiments. This work was
37 supported by the Dr. Miriam and Sheldon G. Adelson Medical Foundation (M.V.S. and
38 T.J.D.), the US National Institutes of Health (NS084030 to M.V.S. and AI112016 to
39 T.J.D.), and the Craig H. Neilsen Foundation (381357 to T.M.O.).
40
41
42
43
44
45
46
47
48
49
50
51
52
53
54
55
56
57
58
59
60
61
62
63
64
65

References

- 1 O'Shea, T. M. *et al.* in *Smart Materials for Tissue Engineering: Applications* (ed Qun Wang) (Royal Society of Chemistry, 2017).
- 2 Mothe, A. J. & Tator, C. H. 2012. Advances in stem cell therapy for spinal cord injury. *The Journal of Clinical Investigation* **122**, 3824-3834.
- 3 Vadivelu, S. *et al.* 2015. NG2+ Progenitors Derived From Embryonic Stem Cells Penetrate Glial Scar and Promote Axonal Outgrowth Into White Matter After Spinal Cord Injury. *Stem Cells Translational Medicine* **4**, 401-411.
- 4 Cao, Q.-I. *et al.* 2001. Pluripotent Stem Cells Engrafted into the Normal or Lesioned Adult Rat Spinal Cord Are Restricted to a Glial Lineage. *Experimental Neurology* **167**, 48-58.
- 5 Wu, S. *et al.* 2001. Migration, integration, and differentiation of hippocampus-derived neurosphere cells after transplantation into injured rat spinal cord. *Neuroscience Letters* **312**, 173-176.
- 6 Lu, P. *et al.* 2012. Long-Distance Growth and Connectivity of Neural Stem Cells after Severe Spinal Cord Injury. *Cell* **150**, 1264-1273.
- 7 Nori, S. *et al.* 2011. Grafted human-induced pluripotent stem-cell derived neurospheres promote motor functional recovery after spinal cord injury in mice. *Proceedings of the National Academy of Sciences* **108**, 16825-16830.
- 8 Falkner, S. *et al.* 2016. Transplanted embryonic neurons integrate into adult neocortical circuits. *Nature* **539**, 248.
- 9 Hallett, Penelope J. *et al.* 2015. Successful Function of Autologous iPSC-Derived Dopamine Neurons following Transplantation in a Non-Human Primate Model of Parkinson's Disease. *Cell Stem Cell* **16**, 269-274.
- 10 Assinck, P., Duncan, G. J., Hilton, B. J., Plemel, J. R. & Tetzlaff, W. 2017. Cell transplantation therapy for spinal cord injury. *Nature Neuroscience* **20**, 637.
- 11 Nishimura, S. *et al.* 2013. Time-dependent changes in the microenvironment of injured spinal cord affects the therapeutic potential of neural stem cell transplantation for spinal cord injury. *Molecular Brain* **6**.
- 12 Piltti, K. M., Salazar, D. L., Uchida, N., Cummings, B. J. & Anderson, A. J. 2013. Safety of epicenter versus intact parenchyma as a transplantation site for human neural stem cells for spinal cord injury therapy. *Stem Cells Transl Med* **2**, 204-216.
- 13 Steward, O., Sharp, K. G., Yee, K. M., Hatch, M. N. & Bonner, J. F. 2014. Characterization of Ectopic Colonies That Form in Widespread Areas of the Nervous System with Neural Stem Cell Transplants into the Site of a Severe Spinal Cord Injury. *The Journal of Neuroscience* **34**, 14013-14021.
- 14 Tuszynski, Mark H. *et al.* 2014. Neural Stem Cell Dissemination after Grafting to CNS Injury Sites. *Cell* **156**, 388-389.
- 15 Kadoya, K. *et al.* 2016. Spinal cord reconstitution with homologous neural grafts enables robust corticospinal regeneration. *Nature Medicine* **22**, 479-487.
- 16 Lu, P. *et al.* 2014. Long-Distance Axonal Growth from Human Induced Pluripotent Stem Cells after Spinal Cord Injury. *Neuron* **83**, 789-796.
- 17 McCreedy, D. A. *et al.* 2014. Survival, differentiation, and migration of high-purity mouse embryonic stem cell-derived progenitor motor neurons in fibrin scaffolds after sub-acute spinal cord injury. *Biomaterials Science* **2**, 1672-1682.

- 1
2
3
4 18 Hoare, T. R. & Kohane, D. S. 2008. Hydrogels in drug delivery: Progress and
5 challenges. *Polymer* **49**, 1993-2007.
6
7 19 Murphy, W. L., McDevitt, T. C. & Engler, A. J. 2014. Materials as stem cell regulators.
8 *Nature Materials* **13**, 547.
9
10 20 Mothe, A. J., Tam, R. Y., Zahir, T., Tator, C. H. & Shoichet, M. S. 2013. Repair of the
11 injured spinal cord by transplantation of neural stem cells in a hyaluronan-based
12 hydrogel. *Biomaterials* **34**, 3775-3783.
13
14 21 Ballios, B. G. *et al.* 2015. A Hyaluronan-Based Injectable Hydrogel Improves the Survival
15 and Integration of Stem Cell Progeny following Transplantation. *Stem Cell Reports* **4**,
16 1031-1045.
17
18 22 Madl, C. M. *et al.* 2017. Maintenance of neural progenitor cell stemness in 3D hydrogels
19 requires matrix remodelling. *Nature Materials* **16**, 1233.
20
21 23 Altunbas, A. & Pochan, D. J. 2012. Peptide-based and polypeptide-based hydrogels for
22 drug delivery and tissue engineering. *Topics in current chemistry* **310**, 135-167.
23
24 24 Deming, T. J. 2005. Polypeptide hydrogels via a unique assembly mechanism. *Soft
25 Matter* **1**, 28-35.
26
27 25 Nowak, A. P. *et al.* 2002. Rapidly recovering hydrogel scaffolds from self-assembling
28 diblock copolypeptide amphiphiles. *Nature* **417**, 424-428.
29
30 26 Anderson, M. A. *et al.* 2016. Astrocyte scar formation aids central nervous system axon
31 regeneration. *Nature* **532**, 195-200.
32
33 27 Yang, C.-Y. *et al.* 2009. Biocompatibility of amphiphilic diblock copolypeptide hydrogels
34 in the central nervous system. *Biomaterials* **30**, 2881-2898.
35
36 28 Zhang, S. *et al.* 2015. Thermoresponsive Copolypeptide Hydrogel Vehicles for Central
37 Nervous System Cell Delivery. *ACS Biomaterials Science & Engineering* **1**, 705-717.
38
39 29 Nicodemus, G. D. & Bryant, S. J. 2008. Cell Encapsulation in Biodegradable Hydrogels
40 for Tissue Engineering Applications. *Tissue Engineering. Part B, Reviews* **14**, 149-165.
41
42 30 Deming, T. J. 2017. Functional Modification of Thioether Groups in Peptides,
43 Polypeptides, and Proteins. *Bioconjugate Chemistry* **28**, 691-700.
44
45 31 Gundlach, H. G., Stein, W. H. & Moore, S. 1959. The nature of the amino acid residues
46 involved in the inactivation of ribonuclease by iodoacetate. *The Journal of biological
47 chemistry* **234**, 1754-1760.
48
49 32 Perlmann, G. E. & Katchalski, E. 1962. Conformation of Poly-L-methionine and Some of
50 its Derivatives in Solution. *Journal of the American Chemical Society* **84**, 452-457.
51
52 33 Kramer, J. R. & Deming, T. J. 2012. Preparation of Multifunctional and Multireactive
53 Polypeptides via Methionine Alkylation. *Biomacromolecules* **13**, 1719-1723.
54
55 34 Kim, G., Weiss, S. J. & Levine, R. L. 2014. Methionine Oxidation and Reduction in
56 Proteins. *Biochimica et biophysica acta* **1840**, 10.1016/j.bbagen.2013.1004.1038.
57
58 35 Brot, N. & Weissbach, H. 1982. The biochemistry of methionine sulfoxide residues in
59 proteins. *Trends in Biochemical Sciences* **7**, 137-139.
60
61 36 Vogt, W. 1995. Oxidation of methionyl residues in proteins: tools, targets, and reversal.
62 *Free radical biology & medicine* **18**, 93-105.
63
64 37 Aiba, S.-I., Minoura, N. & Fujiwara, Y. 1982. Directional permeability of asymmetrically
65 oxidized poly(L-methionine) film to oxygen dissolved in water. *Journal of Applied
Polymer Science* **27**, 1409-1411.

- 1
2
3
4 38 Minoura, N., Fujiwara, Y. & Nakagawa, T. 1978. Permeability of poly-L-methionine
5 membrane and its oxidized membrane to water vapor. *Journal of Applied Polymer*
6 *Science* **22**, 1593-1605.
7
8 39 Pitha, J., Szente, L. & Greenberg, J. 1983. Poly-L-methionine Sulfoxide: A Biologically
9 Inert Analogue of Dimethyl Sulfoxide with Solubilizing Potency. *Journal of*
10 *Pharmaceutical Sciences* **72**, 665-668.
11 40 Rodriguez, A. R., Kramer, J. R. & Deming, T. J. 2013. Enzyme-Triggered Cargo Release
12 from Methionine Sulfoxide Containing Copolypeptide Vesicles. *Biomacromolecules* **14**,
13 3610-3614.
14
15 41 Yamada, S., Ikkyu, K., Iso, K., Goto, M. & Endo, T. 2015. Facile synthesis of
16 polymethionine oxides through polycondensation of activated urethane derivative of
17 [small alpha]-amino acid and their application to antifouling polymer against proteins and
18 cells. *Polymer Chemistry* **6**, 1838-1845.
19
20 42 Chapman, R. G. *et al.* 2000. Surveying for Surfaces that Resist the Adsorption of
21 Proteins. *Journal of the American Chemical Society* **122**, 8303-8304.
22 43 Ostuni, E., Chapman, R. G., Holmlin, R. E., Takayama, S. & Whitesides, G. M. 2001. A
23 Survey of Structure–Property Relationships of Surfaces that Resist the Adsorption of
24 Protein. *Langmuir* **17**, 5605-5620.
25
26 44 Gombotz, W. R., Guanghui, W., Horbett, T. A. & Hoffman, A. S. 1991. Protein adsorption
27 to poly(ethylene oxide) surfaces. *Journal of Biomedical Materials Research* **25**, 1547-
28 1562.
29
30 45 Deng, L., Mrksich, M. & Whitesides, G. M. 1996. Self-Assembled Monolayers of
31 Alkanethiolates Presenting Tri(propylene sulfoxide) Groups Resist the Adsorption of
32 Protein. *Journal of the American Chemical Society* **118**, 5136-5137.
33 46 Luk, Y.-Y., Kato, M. & Mrksich, M. 2000. Self-Assembled Monolayers of Alkanethiolates
34 Presenting Mannitol Groups Are Inert to Protein Adsorption and Cell Attachment.
35 *Langmuir* **16**, 9604-9608.
36
37 47 Mukkamala, R., Kushner, A. M. & Bertozzi, C. R. in *Polymer Gels* Vol. 833 ACS
38 *Symposium Series* Ch. 11, 163-174 (American Chemical Society, 2002).
39 48 Brot, N., Weissbach, L., Werth, J. & Weissbach, H. 1981. Enzymatic reduction of
40 protein-bound methionine sulfoxide. *Proceedings of the National Academy of Sciences*
41 **78**, 2155-2158.
42
43 49 Kramer, J. R. & Deming, T. J. 2010. General Method for Purification of α -Amino acid-N-
44 carboxyanhydrides Using Flash Chromatography. *Biomacromolecules* **11**, 3668-3672.
45 50 Deming, T. J. 1999. Cobalt and Iron Initiators for the Controlled Polymerization of α -
46 Amino Acid-N-Carboxyanhydrides. *Macromolecules* **32**, 4500-4502.
47
48 51 Hernández, J. R. & Klok, H.-A. 2003. Synthesis and ring-opening (co)polymerization of
49 L-lysine N-carboxyanhydrides containing labile side-chain protective groups. *Journal of*
50 *Polymer Science Part A: Polymer Chemistry* **41**, 1167-1187.
51
52 52 Mavroggiorgis, D. *et al.* 2014. Controlled polymerization of histidine and synthesis of well-
53 defined stimuli responsive polymers. Elucidation of the structure-aggregation relationship
54 of this highly multifunctional material. *Polymer Chemistry* **5**, 6256-6278.
55 53 Sun, Y. *et al.* 2017. Conformation-Directed Formation of Self-Healing Diblock
56 Copolypeptide Hydrogels via Polyion Complexation. *Journal of the American Chemical*
57 *Society* **139**, 15114-15121.
58
59 54 Sanz, E. *et al.* 2009. Cell-type-specific isolation of ribosome-associated mRNA from
60 complex tissues. *Proceedings of the National Academy of Sciences* **106**, 13939-13944.
61
62
63
64
65

- 1
2
3
4 55 Brown, C. R., Butts, J. C., McCreedy, D. A. & Sakiyama-Elbert, S. E. 2014. Generation
5 of V2a Interneurons from Mouse Embryonic Stem Cells. *Stem Cells and Development*
6 **23**, 1765-1776.
7
8 56 Roybon, L. *et al.* 2013. Human Stem Cell-Derived Spinal Cord Astrocytes with Defined
9 Mature or Reactive Phenotypes. *Cell Reports* **4**, 1035-1048.
10
11 57 Wichterle, H., Lieberam, I., Porter, J. A. & Jessell, T. M. 2002. Directed Differentiation of
12 Embryonic Stem Cells into Motor Neurons. *Cell* **110**, 385-397.
13
14 58 Krencik, R., Weick, J. P., Liu, Y., Zhang, Z.-J. & Zhang, S.-C. 2011. Specification of
15 transplantable astroglial subtypes from human pluripotent stem cells. *Nature*
16 *Biotechnology* **29**, 528.
17
18 59 Lutolf, M. P. & Hubbell, J. A. 2005. Synthetic biomaterials as instructive extracellular
19 microenvironments for morphogenesis in tissue engineering. *Nature Biotechnology* **23**,
20 47.
21
22 60 Guilak, F. *et al.* 2009. Control of Stem Cell Fate by Physical Interactions with the
23 Extracellular Matrix. *Cell Stem Cell* **5**, 17-26.
24
25 61 Teixeira, A. I., Duckworth, J. K. & Hermanson, O. 2007. Getting the right stuff:
26 Controlling neural stem cell state and fate in vivo and in vitro with biomaterials. *Cell*
27 *Research* **17**, 56.
28
29 62 Khakh, B. S. & Sofroniew, M. V. 2015. Diversity of astrocyte functions and phenotypes in
30 neural circuits. *Nature neuroscience* **18**, 942-952.
31
32 63 Norris, C. & Kalil, K. 1991. Guidance of callosal axons by radial glia in the developing
33 cerebral cortex. *The Journal of Neuroscience* **11**, 3481-3492.
34
35 64 Hasegawa, K. *et al.* 2005. Embryonic radial glia bridge spinal cord lesions and promote
36 functional recovery following spinal cord injury. *Experimental Neurology* **193**, 394-410.
37
38 65 Chandrasekaran, A., Avci, H. X., Leist, M., Kobilák, J. & Dinnyés, A. 2016. Astrocyte
39 Differentiation of Human Pluripotent Stem Cells: New Tools for Neurological Disorder
40 Research. *Frontiers in Cellular Neuroscience* **10**, 215.
41
42 66 Chai, H. *et al.* 2017. Neural Circuit-Specialized Astrocytes: Transcriptomic, Proteomic,
43 Morphological, and Functional Evidence. *Neuron* **95**, 531-549.e539.
44
45 67 Carmichael, S. T. 2016. The 3 Rs of Stroke Biology: Radial, Relayed, and Regenerative.
46 *Neurotherapeutics* **13**, 348-359.
47
48 68 O'Shea, T. M., Burda, J. E. & Sofroniew, M. V. 2017. Cell biology of spinal cord injury
49 and repair. *Journal of Clinical Investigation* **127**, 3259-3270.
50
51
52
53
54
55
56
57
58
59
60
61
62
63
64
65

Figures

Injectable polypeptide hydrogels via methionine modification for neural stem cell delivery

¹A.L. Wollenberg*, ²T. M. O'Shea*, ²J.H. Kim, ³A. Czechanski, ³L.G. Reinholdt, ²M.V. Sofroniew, and ¹T.J. Deming†.

¹ Departments of Bioengineering, Chemistry and Biochemistry, University of California Los Angeles, Los Angeles, California 90095-1600, USA.

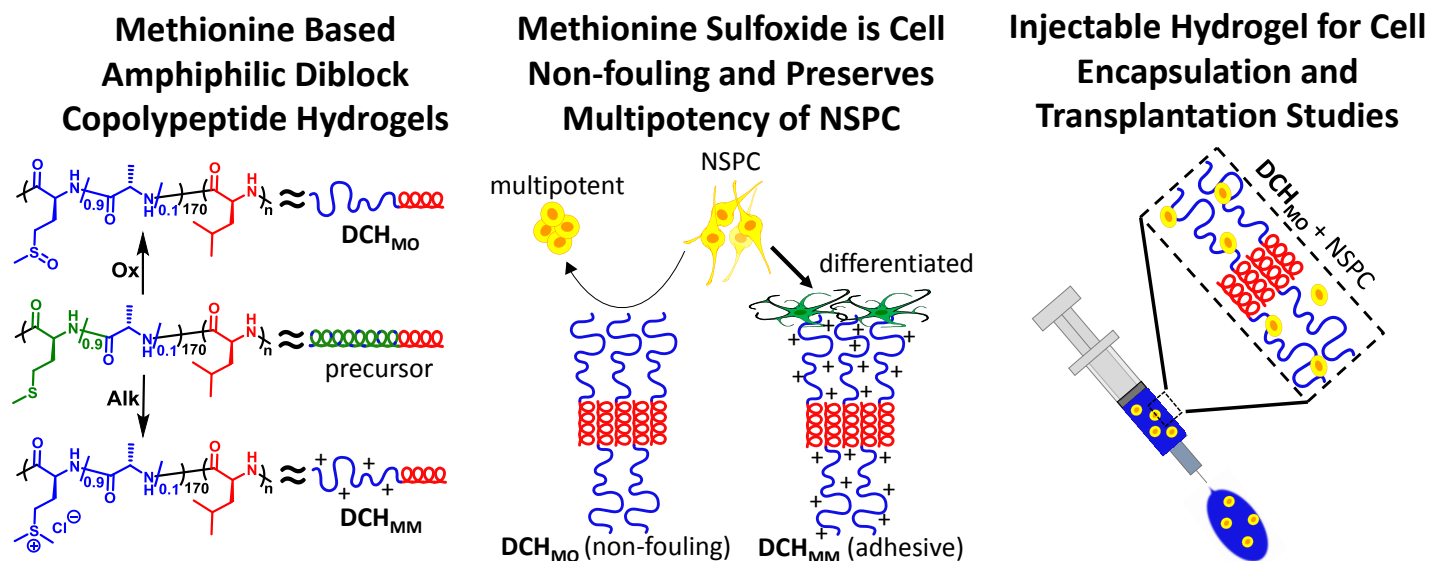
² Department of Neurobiology, David Geffen School of Medicine, University of California, Los Angeles, California 90095-1763, USA.

³ The Jackson Laboratory, Bar Harbor, Maine, 04609, USA.

* These authors contributed equally to this work.

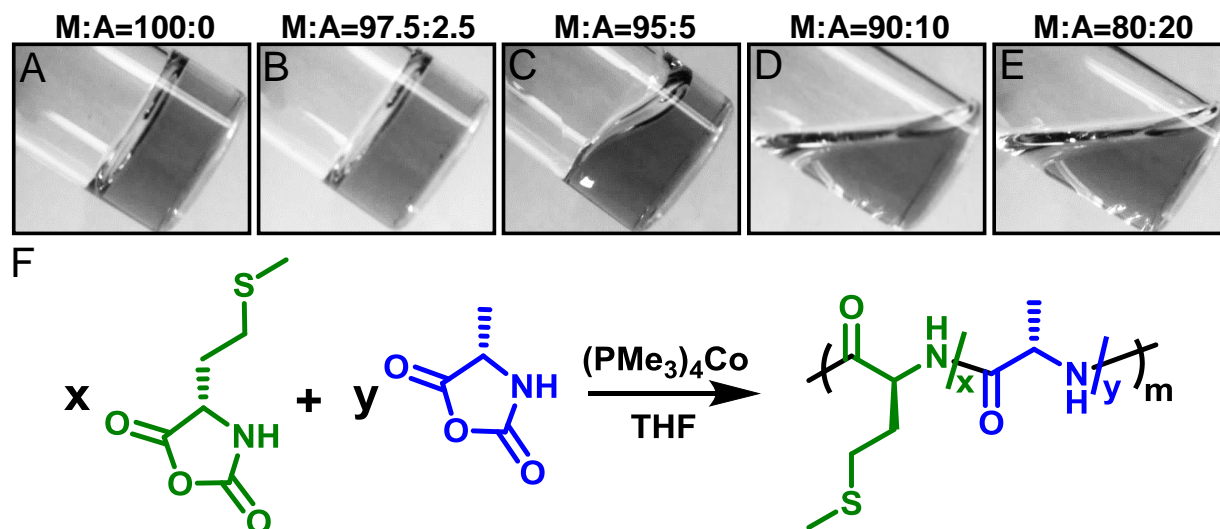
† Corresponding Author

TOC/Graphical Abstract Figure



Graphical Abstract (13" x 5")

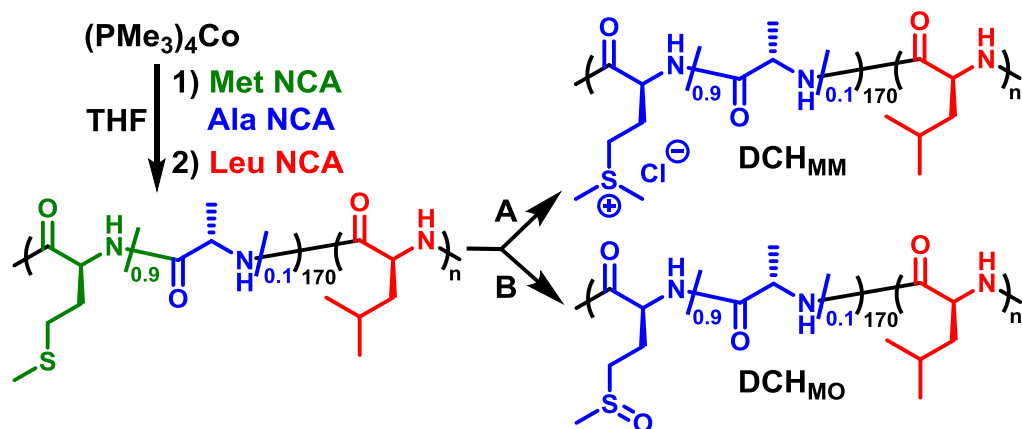
SCHEME 1



Scheme 1: Synthesis of MA statistical copolymers. Copolymerization of L-methionine NCA and L-alanine NCA with $\text{Co}(\text{PMe}_3)_4$ initiator to give MA copolymers in THF with a total NCA concentration of 50 mg/mL and total monomer to initiator ratio of 60:1. Images of reaction mixtures after complete monomer consumption were taken 30 seconds after tilting the vial to evaluate solution viscosity. **A)** M:A molar ratio = 100:0. **B)** M:A molar ratio = 97.5:2.5. **C)** M:A molar ratio = 95:5. **D)** M:A molar ratio = 90:10. **E)** M:A molar ratio = 80:20. **F)** Reaction scheme for the copolymerization of L-methionine and L-alanine NCAs. x = mole fraction M. y = mole fraction A. m = degree of polymerization.

[Designated as a full page width (two column) figure]

SCHEME 2



Scheme 2: Synthesis of modified methionine amphiphilic diblock copolypeptides: cationic $(\text{M}^{\text{M}}\text{A})_{170}\text{L}_n$ (DCH_{MM}) and nonionic $(\text{M}^{\text{O}}\text{A})_{170}\text{L}_n$ (DCH_{MO}). Reaction conditions: (A) MeI, H_2O , 20 °C, 5 d ; (B) TBHP, CSA, H_2O , 20 °C 1 d.

[Designated as a half page width (single column) figure]

TABLE 1

	Sample	M_w/M_n^a	Composition ^b	Yield ^c (%)	Functional Modification ^d (%)
DCH _{MO}	M ^O ₁₇₀ L ₂₃	1.28	M ^O ₁₇₆ L ₂₃	88.1	100
	(M ^O A) ₁₇₀ L ₁₂	1.44	(M ^O A) ₁₇₅ L ₁₂	84.3	100
	(M ^O A) ₁₇₀ L ₁₇	1.44	(M ^O A) ₁₆₄ L ₁₇	85.2	100
	(M ^O A) ₁₇₀ L ₂₄	1.44	(M ^O A) ₁₇₁ L ₂₄	84.6	100
	(M ^O A) ₁₇₀ L ₂₈	1.36	(M ^O A) ₁₆₇ L ₂₈	84.1	100
	(M ^O A) ₁₇₀ L ₃₃	1.33	(M ^O A) ₁₇₂ L ₃₃	85.6	100
	(M ^O A) ₁₇₀ L ₃₉	1.41	(M ^O A) ₁₆₄ L ₃₉	86.5	100
DCH _{MM}	M ^M ₁₇₀ L ₂₄	1.34	M ^M ₁₇₆ L ₂₄	88.7	98
	(M ^M A) ₁₇₀ L ₁₂	1.44	(M ^M A) ₁₇₉ L ₁₂	90.3	99
	(M ^M A) ₁₇₀ L ₁₇	1.35	(M ^M A) ₁₇₉ L ₁₇	88.8	99
	(M ^M A) ₁₇₀ L ₂₃	1.33	(M ^M A) ₁₇₈ L ₂₃	93.4	99
	(M ^M A) ₁₇₀ L ₂₇	1.34	(M ^M A) ₁₆₅ L ₂₇	92.7	99
	(M ^M A) ₁₇₀ L ₃₃	1.29	(M ^M A) ₁₆₅ L ₃₃	93.4	99
	(M ^M A) ₁₇₀ L ₃₆	1.25	(M ^M A) ₁₆₇ L ₃₆	93.4	98

Table 1: Copolymerization data for DCH_{MO} and DCH_{MM}. ^aDispersity values for (MA)_m copolypeptides were determined by GPC/LS. ^bAmino acid compositions of diblock copolypeptides were determined by ¹H NMR integrations. Degree of polymerization of initial (MA)_m segment was determined by end-group analysis using ¹H NMR. ^cOverall isolated yield of diblock copolypeptide after oxidation or alkylation of methionine residues. ^dPercent functionalization after oxidation or alkylation reactions was determined using ¹H NMR.

[Designated as a full page width (two column) table]

TABLE 2

	Sample	1 wt %	2 wt %	3 wt %	5 wt %	7 wt %	9 wt %
DCH_{MO}	M ^O ₁₇₀ L ₂₃						
	(M ^O A) ₁₇₀ L ₁₂						
	(M ^O A) ₁₇₀ L ₁₇						
	(M ^O A) ₁₇₀ L ₂₄						
	(M ^O A) ₁₇₀ L ₂₈						
	(M ^O A) ₁₇₀ L ₃₃						
	(M ^O A) ₁₇₀ L ₃₉						
DCH_{MM}	M ^M ₁₇₀ L ₂₄						
	(M ^{MA}) ₁₇₀ L ₁₂						
	(M ^{MA}) ₁₇₀ L ₁₇						
	(M ^{MA}) ₁₇₀ L ₂₃						
	(M ^{MA}) ₁₇₀ L ₂₇						
	(M ^{MA}) ₁₇₀ L ₃₃						
	(M ^{MA}) ₁₇₀ L ₃₆						

Table 2: Hydrogel formation of DCH_{MO} and DCH_{MM}. Properties of DCH_{MO} and DCH_{MM} samples after dispersion in DI H₂O at different concentrations. Samples were found to be either clear liquids (gray box), clear hydrogels (white box), or opaque hydrogels (*).

[Designated as a full page width (two column) table]

FIGURE 1

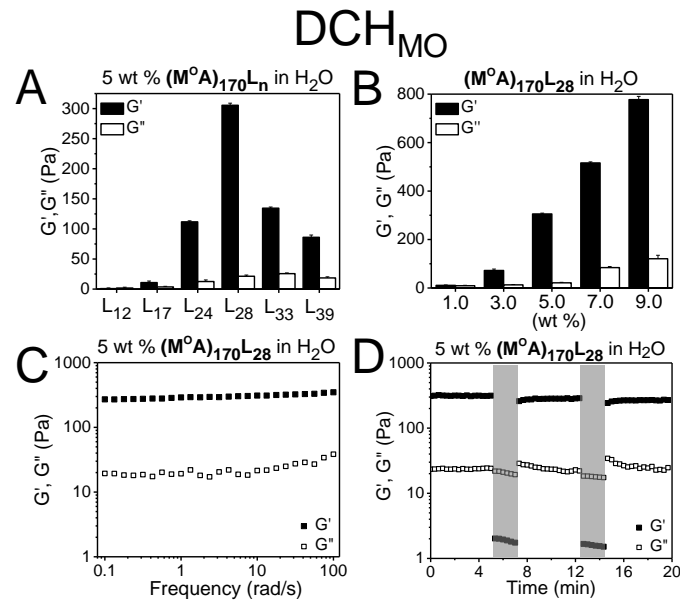


Figure 1: DCH_{MO} mechanical properties evaluated by dynamic rheology. A) Storage modulus, G' (Pa, black) and loss modulus, G'' (Pa, white) for (M^OA)₁₇₀L_n samples of different hydrophobic segment lengths (n = 12, 17, 24, 28, 33, and 39). All samples (5 wt %) were prepared in DI water at 25 °C. **B)** G' (Pa, black) and G'' (Pa, white) for (M^OA)₁₇₀L₂₈ at different concentrations in DI water at 25 °C. For **A)** and **B)** all G' and G'' values were measured at an angular frequency of 10 rad/s and a percent strain of 0.5. Error bars represent the standard deviation for n = 3. **C)** G' (Pa, filled squares) and G'' (Pa, open squares) for (M^OA)₁₇₀L₂₈ at 5 wt % in DI water. G' and G'' values were measured over an angular frequency range of 0.1 to 100 rad/s at a percent strain of 0.5. **D)** Recovery of a 5 wt % (M^OA)₁₇₀L₂₈ hydrogel in DI water over time (G', filled squares; G'', open squares) after application of stepwise large-amplitude oscillatory breakdown (gray area, percent strain of 1000 at 10 rad/s for 120 s) followed by low-amplitude linear recovery (white area, percent strain of 0.5 at 10 rad/s for 300 s).

[Designated as a half page width (single column) figure]

FIGURE 2

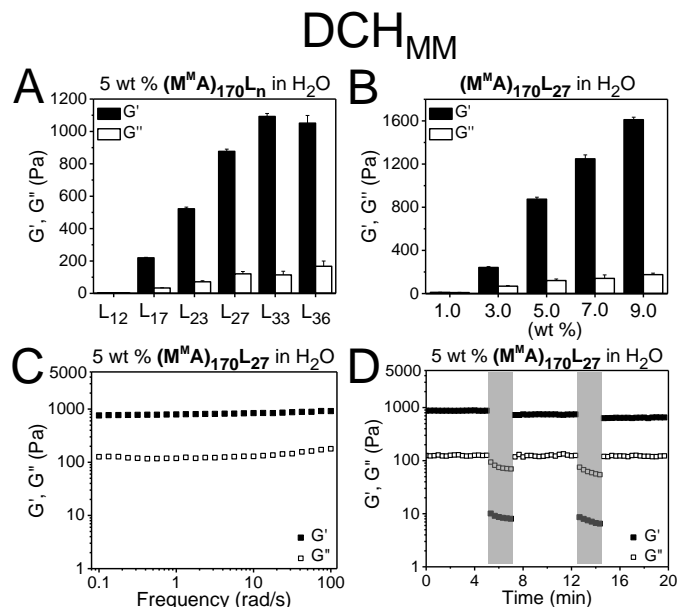


Figure 2: DCH_{MM} mechanical properties evaluated by dynamic rheology. A) Storage modulus, G' (Pa, black) and loss modulus, G'' (Pa, white) for $(M^M A)_{170}L_n$ samples of different hydrophobic segment lengths ($n = 12, 17, 23, 27, 33,$ and 36). All samples (5 wt %) were prepared in DI water at 25 °C. **B)** G' (Pa, black) and G'' (Pa, white) for $(M^M A)_{170}L_{27}$ at different concentrations in DI water at 25 °C. For **A)** and **B)** all G' and G'' values were measured at an angular frequency of 10 rad/s and a percent strain of 0.5. Error bars represent the standard deviation for $n = 3$. **C)** G' (Pa, filled squares) and G'' (Pa, open squares) for $(M^M A)_{170}L_{27}$ at 5 wt % in DI water. G' and G'' values were measured over an angular frequency range of 0.1 to 100 rad/s at a percent strain of 0.5. **D)** Recovery of a 5 wt % $(M^M A)_{170}L_{27}$ hydrogel in DI water over time (G' , filled squares; G'' , open squares) after application of stepwise large-amplitude oscillatory breakdown (gray area, percent strain of 1000 at 10 rad/s for 120 s) followed by low-amplitude linear recovery (white area, percent strain of 0.5 at 10 rad/s for 300 s).

[Designated as a half page width (single column) figure]

FIGURE 3

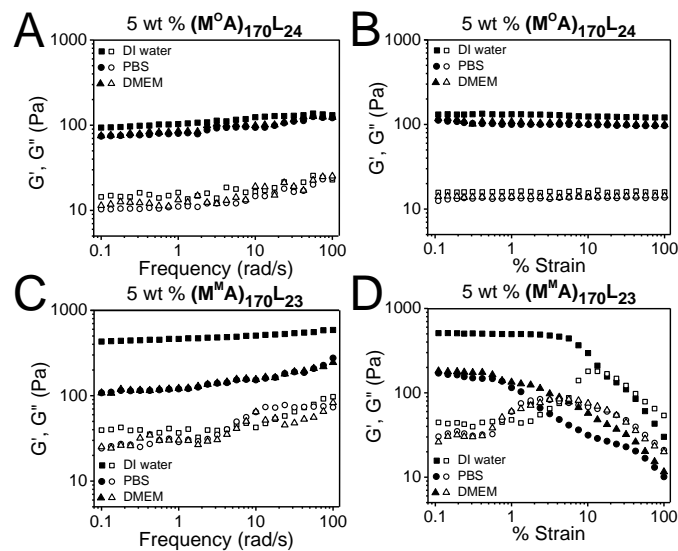


Figure 3: Effects of ionic media on DCH mechanical properties. DCH_{MO} and DCH_{MM} properties in DI water (squares), 1x PBS (circles), or DMEM (triangles). **A)** Storage modulus, G' (Pa, filled symbols), and loss modulus, G'' (Pa, open symbols) versus frequency for 5 wt % $(M^O A)_{170L24}$ at 25 °C in different media. **B)** G' (Pa, filled symbols), and G'' (Pa, open symbols) versus percent strain for 5 wt % $(M^O A)_{170L24}$ at 25 °C in different media. **C)** G' (Pa, filled symbols), and G'' (Pa, open symbols) versus frequency for 5 wt % $(M^M A)_{170L23}$ at 25 °C in different media. **D)** G' (Pa, filled symbols), and G'' (Pa, open symbols) versus percent strain for 5 wt % $(M^M A)_{170L23}$ at 25 °C in different media. For **A)** and **C)** G' and G'' values were measured over an angular frequency of 0.1 to 100 rad/s at a percent strain of 0.5. For **B)** and **D)** G' and G'' values were measured at an angular frequency of 10 rad/s over a percent strain of 0.1 to 100.

[Designated as a half page width (single column) figure]

FIGURE 4

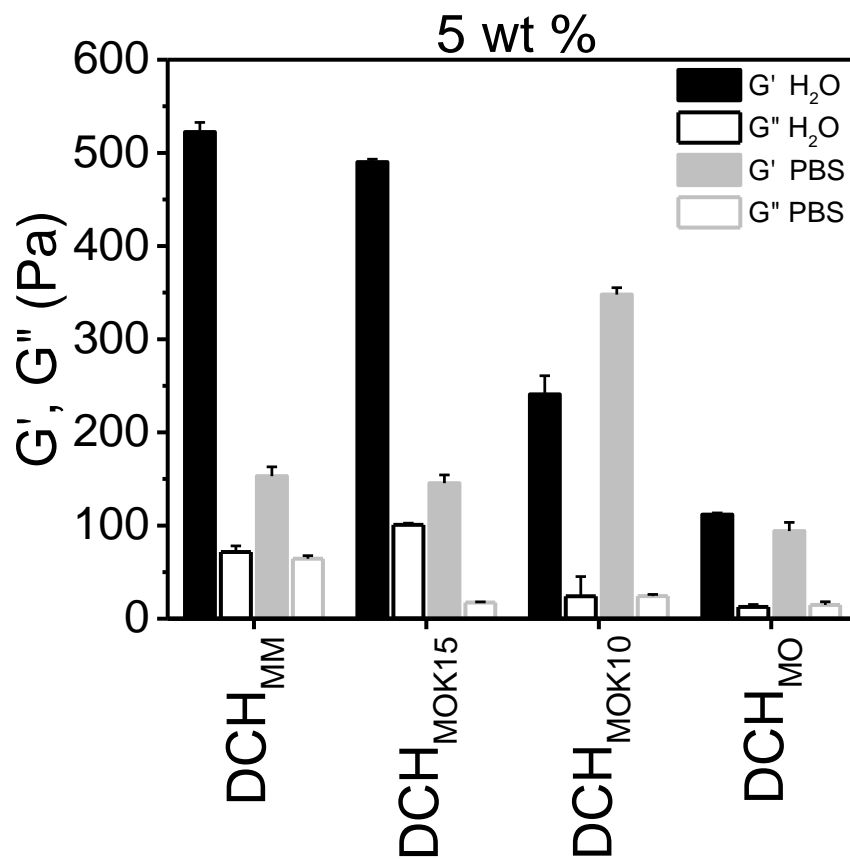


Figure 4: Effect of amino acid composition on DCH mechanical properties. Comparison of mechanical properties for DCH_{MM} ((M^MA)₁₇₀L₂₃), DCH_{MO} ((M^OA)₁₇₀L₂₄), DCH_{MOK10} ((M^O_{0.90}K_{0.10})₁₇₀L₂₃), and DCH_{MOK15} ((M^O_{0.85}K_{0.15})₁₇₀L₂₃) hydrogels. Hydrogels were prepared in either DI water (black bars) or 1x PBS (gray bars) at 5 wt %. Storage modulus G' (Pa, filled bars) and loss modulus G'' (Pa, open bars) were measured at an angular frequency of 10 rad/s and a percent strain of 0.5 at 25 °C. Error bars represent the standard deviations for n = 3.

[Designated as a half page width (single column) figure]

FIGURE 5

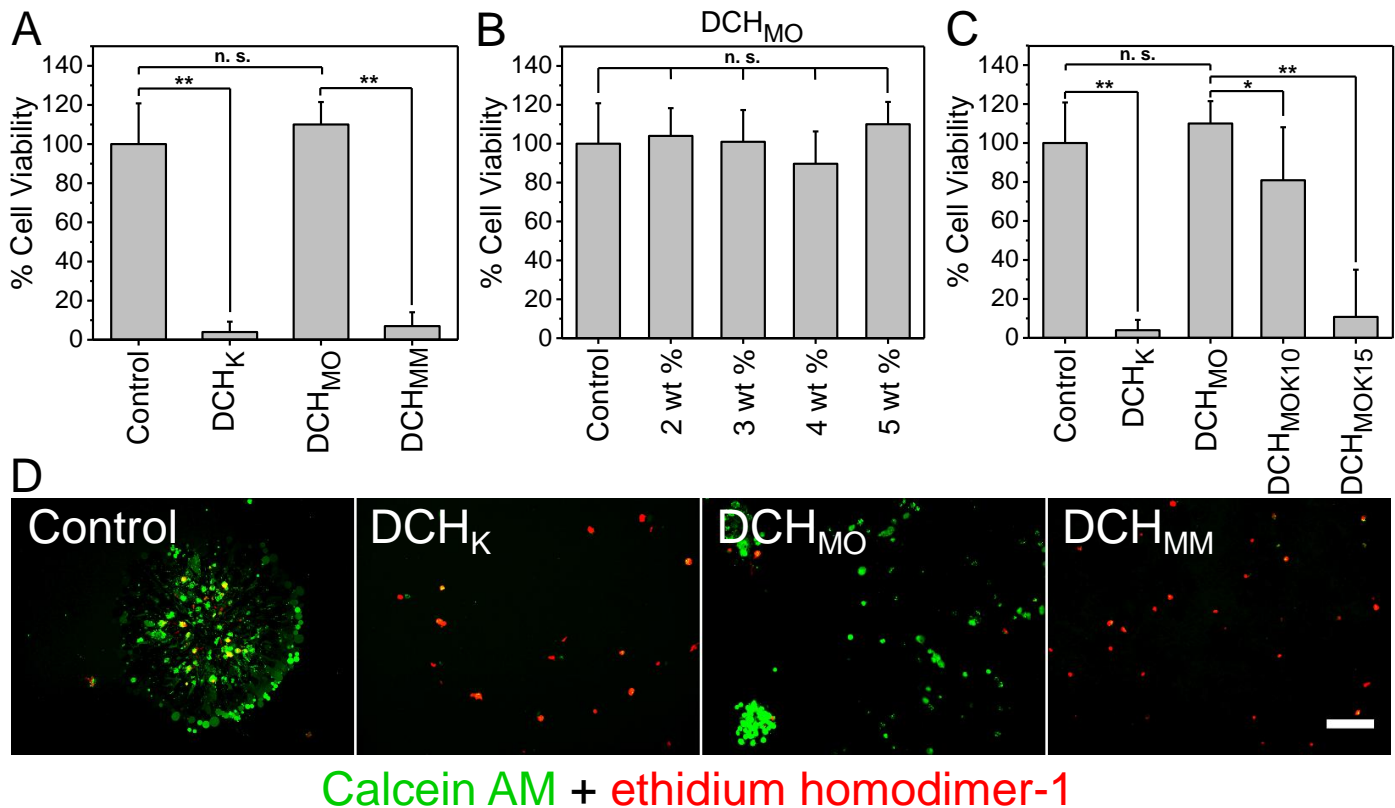


Figure 5: NSPC viability in Met based DCH. A-C) Quantification of cell viability of NSPCs in hydrogels demonstrates that DCH_{MO} is non-cytotoxic towards suspended NSPC across 2-5 wt% while cationic polypeptides are cytotoxic in a charge density dependent manner. **D)** Images of Calcein AM (Green - Live cell marker) and ethidium homodimer-1 (Red - dead cell marker) staining for NSPCs in various hydrogel formulations. Scale bar: 100 μ m. Error bars are standard deviation of $n = 15$. Statistical tests: One-way Anova in **B)** and Welch's t-test in **A)** & **C)** were applied for comparison of means. P-values: * < 0.002 and ** < 0.0001.

[Designated as a full page width (two column) figure]

FIGURE 6

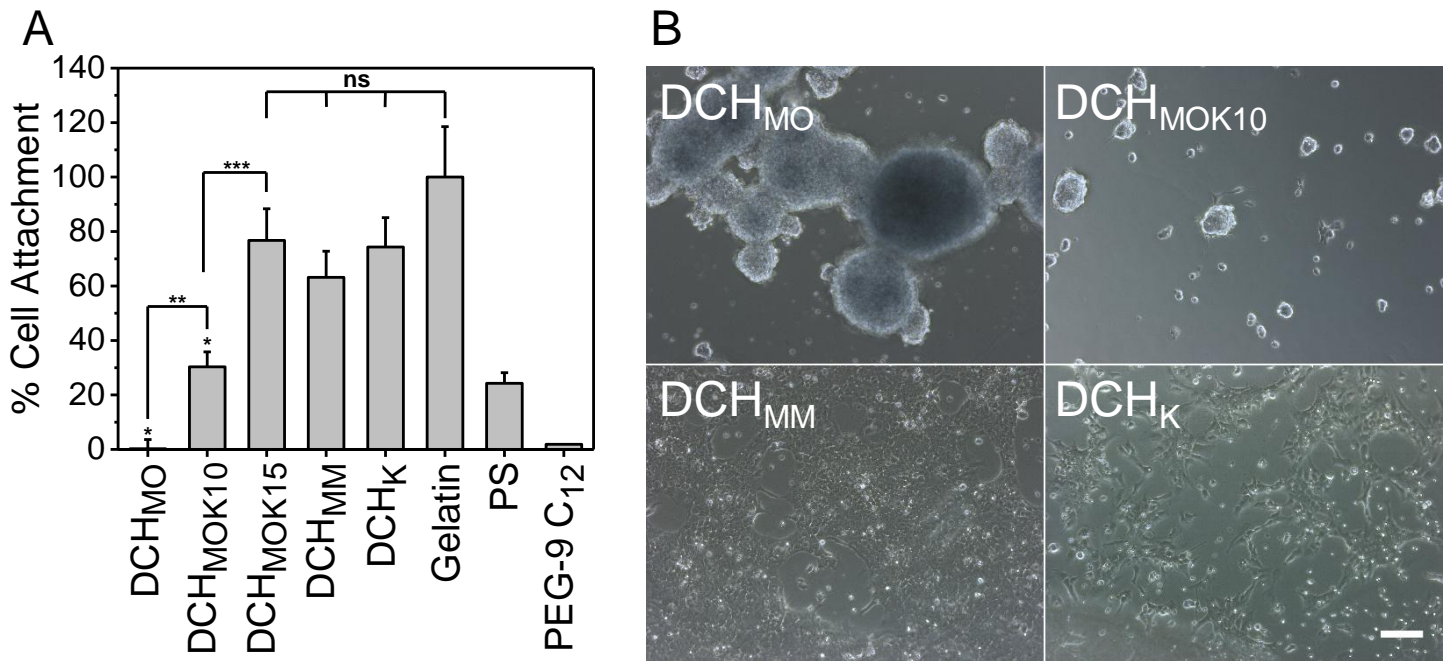


Figure 6: NSPC adhesion to Met based DCH. Untreated polystyrene 96 well plates or hydrophobic glass slides were modified with different samples followed by seeding of NSPC. **A)** Quantification of NSPC attachment, as measured by fluorescent microplate measurements of Calcein AM staining, demonstrates the non-fouling properties of DCH_{MO} and the effect of polypeptide cationic charge on cell adhesion. Error bars are standard error of $n = 12$. Welch's t-tests were applied for the comparisons of individual DCH means compared to each other or compared to the Gelatin control. P-values: * < 0.003; ** < 0.002; *** < 0.0024. **B)** Brightfield microscope images of live NSPC on polypeptide coated hydrophobic glass substrates. NSPC seeded on DCH_{MO} do not adhere to the surface and instead form large multicellular aggregates. Scale bar: 100 μ m.

[Designated as a full page width (two column) figure]

FIGURE 7

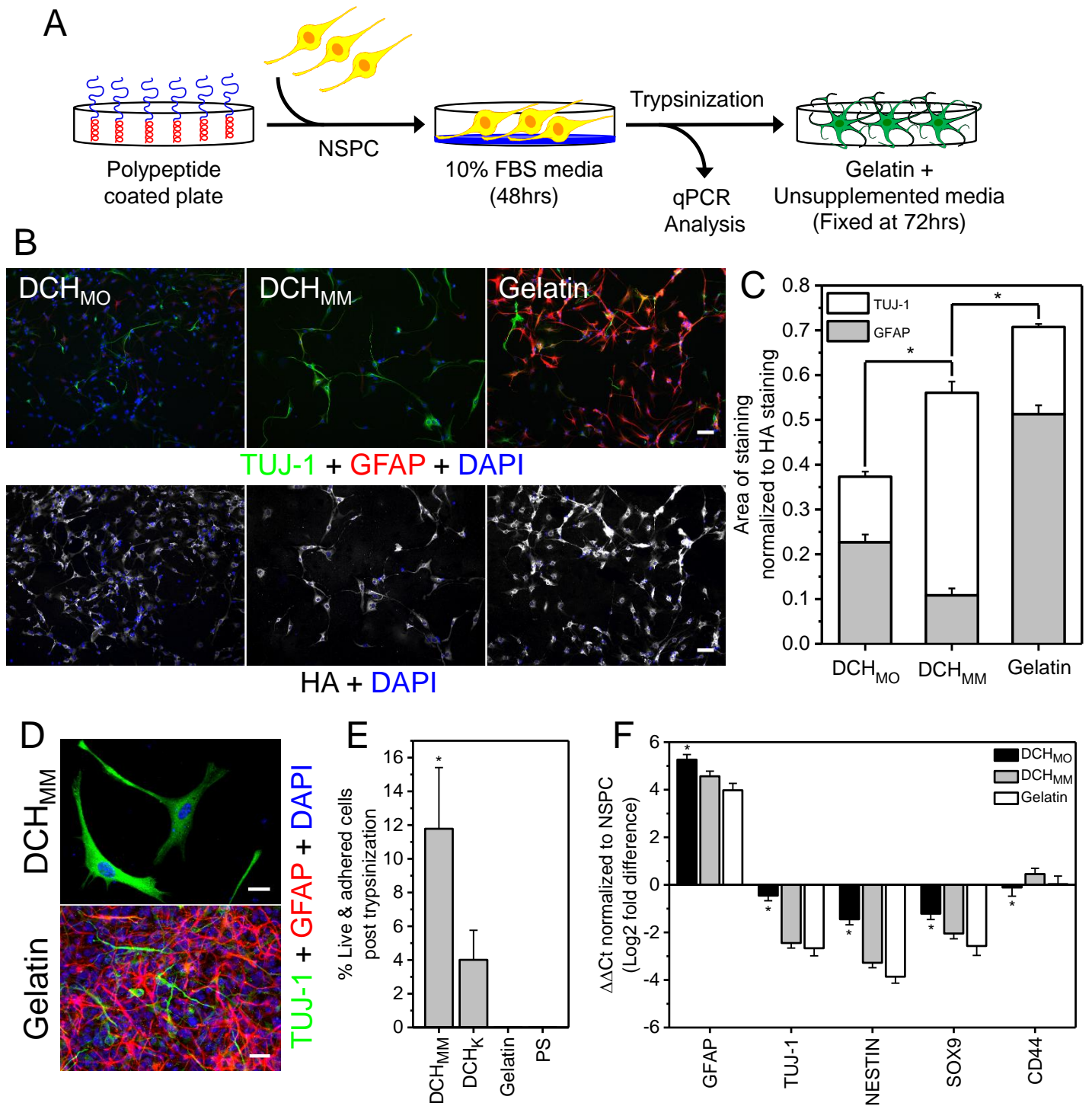


Figure 7: NSPC differentiation with Met Based DCH. **A)** Schematic outlining the *in vitro* culture assay to evaluate NSPC differentiation on various coated substrates. **B)** Immuno-histochemical staining of pan neuronal (TUJ-1-Green) and astrocyte (GFAP-Red) as well as whole cell staining by HA to evaluate NSPC differentiation on DCH_{MO}, DCH_{MM}, and Gelatin (Scale bar: 50µm). **C)** Quantification of Immunohistochemical staining for the different substrates reveals that DCH_{MO} promotes preserved NSPC multipotency. (n=28-30 images per group from 5 unique slides, error bars are represented as standard error or means. * P-value < 0.001). **D)** Immunohistochemical staining of TUJ-1 and GFAP on DCH_{MM} and Gelatin at the conclusion of FBS treatment (Scale bar: 20µm). **E)** Quantification of adhered viable cells remaining on coated surfaces after trypsinization reveals stronger cell attachment to DCH_{MM} compared to Gelatin (*P-value < 0.01). **F)** qPCR analysis of neural genes in NSPC samples seeded for 48hours on DCH_{MO}, DCH_{MM}, and Gelatin substrates in FBS containing medium (n=4, cDNA for each sample derived from mRNA collected by pooling of mRNA collected from cells from 3 unique experiments, * P-value < 0.03). Welch's t-tests were applied for the comparison of means throughout Figure 7.

[Designated as a full page width (two column) figure]

FIGURE 8

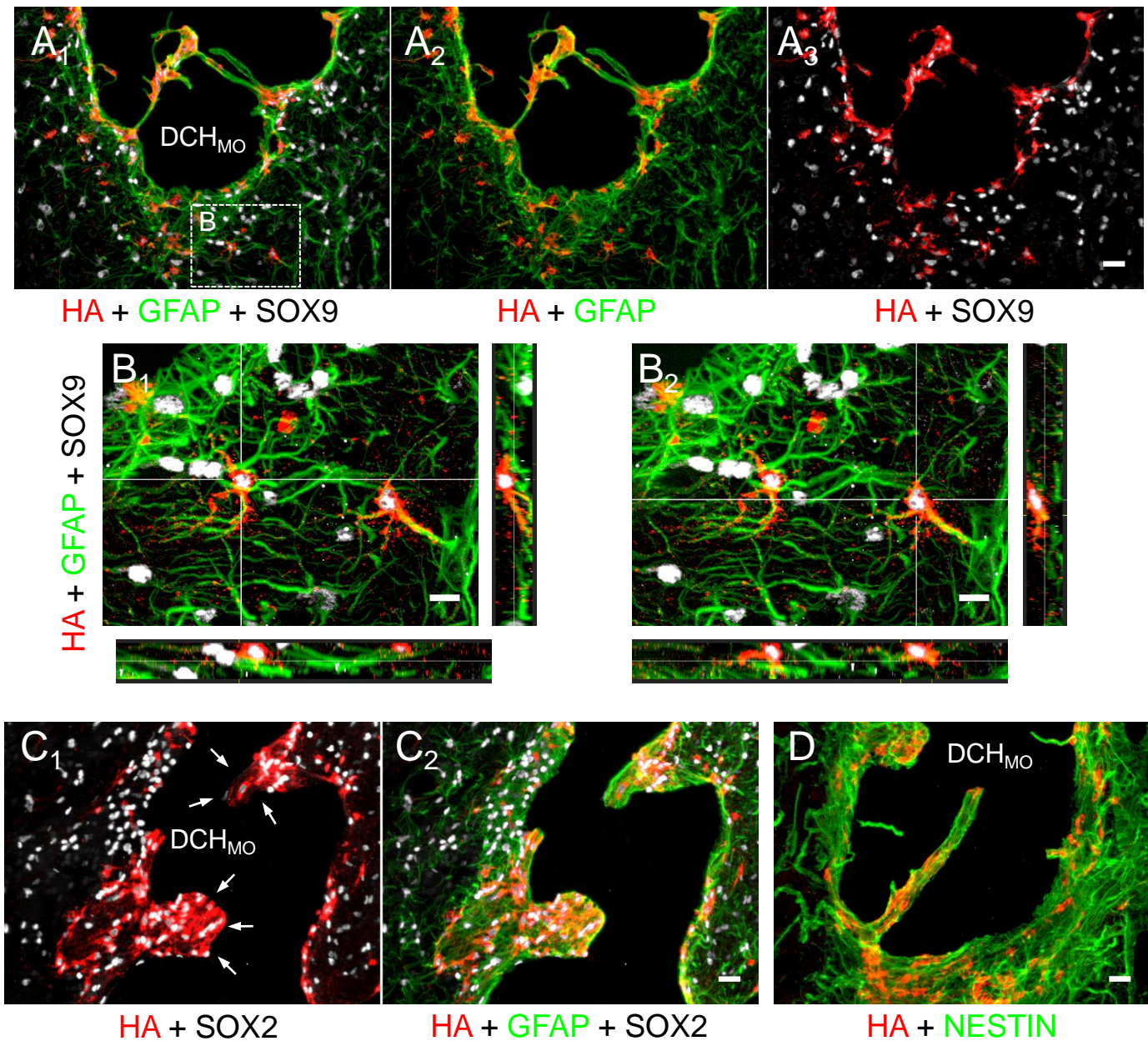


Figure 8: NSPC transplanted into healthy mouse brain using DCH_{MO} vehicle display an immature glial phenotype at 4 weeks. **A)** Immunohistochemical analysis of the DCH_{MO} + NSPC injection zone demonstrates abundant HA positive transplanted cells that robustly express GFAP and SOX9. **B)** High magnification and three-dimensional orthogonal-image of two unique HA positive cells that have integrated into healthy neural tissue and have adopted distinct, individual cellular domains. **C)** HA positive cells maintain robust expression of SOX2. Arrows in **C)** indicate transplanted neurospheres that have adhered to the margins of the DCH_{MO} deposit and integrated into host tissue. **D)** HA positive cells maintain robust expression of NESTIN. Scale bars in: **A), C) & D)** are 25 μ m; **B)** is 10 μ m.

[Designated as a full page width (two column) figure]

FIGURE 9

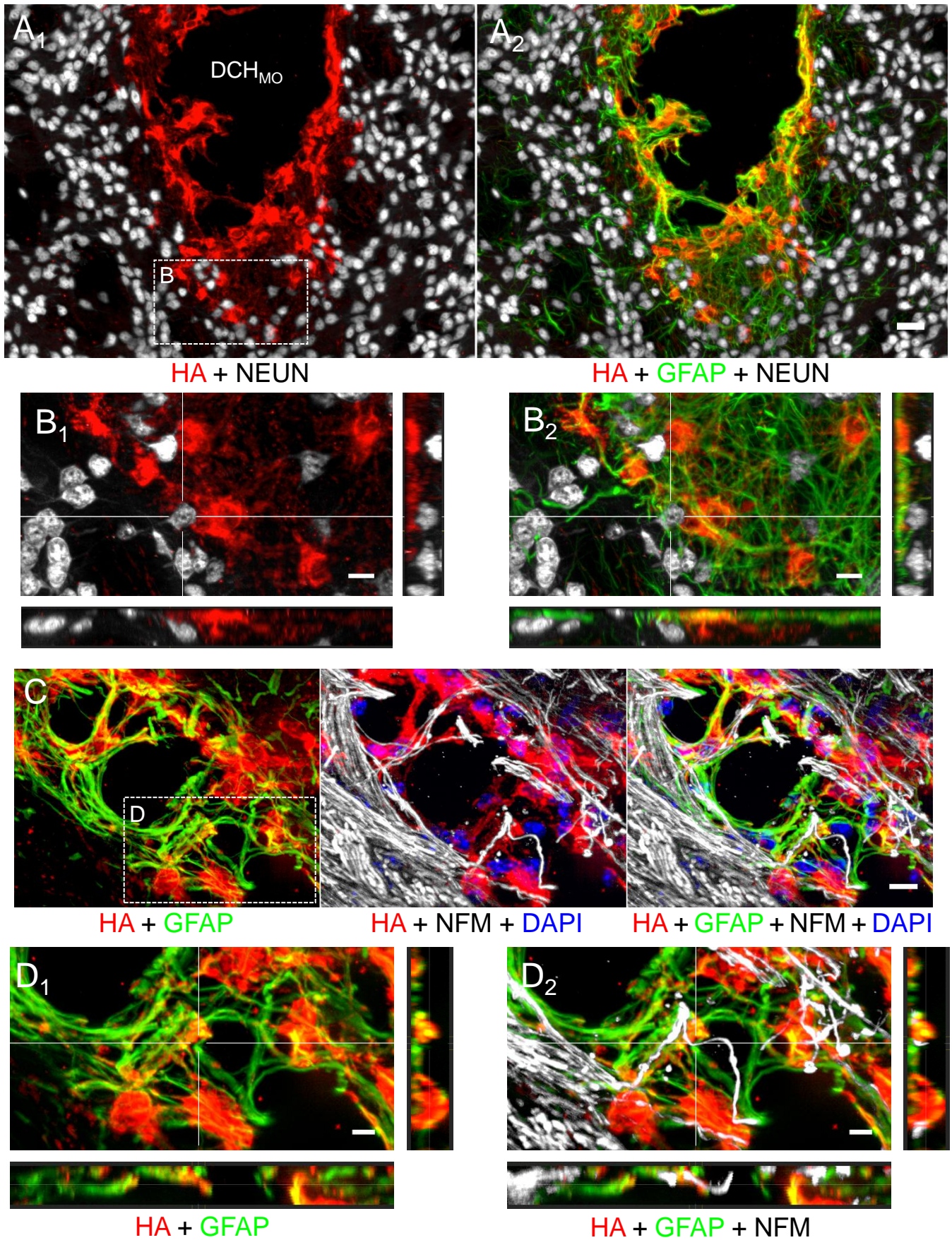
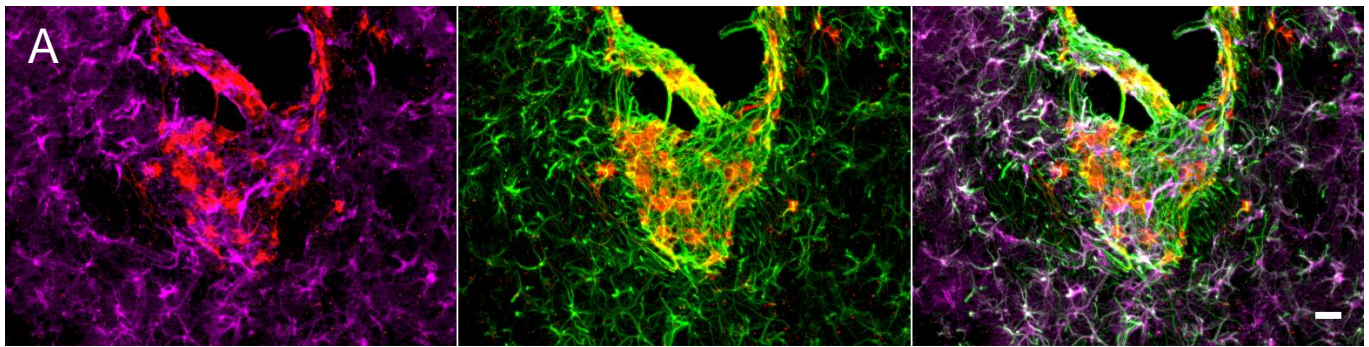


Figure 9: Transplanted NSPC interact with host neurons and provide cellular substrates for host axon growth. A) Immunohistochemical image showing integration of HA positive transplanted cells into host tissue with abundant NEUN positive neurons. **B)** High magnification image of a field from **A)** with a three dimensional orthogonal projection depicting HA positive cells interacting with NEUN positive neurons via GFAP positive cellular projections. **C)** Immunohistochemical image showing HA positive cells providing a cellular substrate for regrowth of axons that have been disrupted as a result of hydrogel injection. The torturous growth projection of the axon stained with NFM is indicative of a newly regrowing or sprouted fiber. **D)** High magnification, three dimensional orthogonal projection showing NFM positive regrowing fibers in contact with a HA positive cells. Scale bars in: **A)** is 25 μm ; **B)** & **C)** are 10 μm ; and **D)** is 5 μm .

[Designated as a full page width (two column) figure]

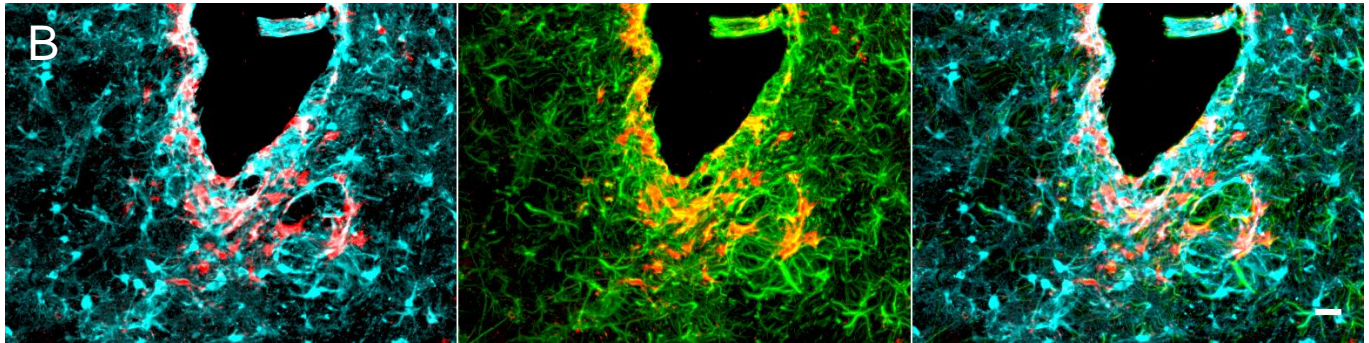
FIGURE 10



HA + ALDH1L1

HA + GFAP

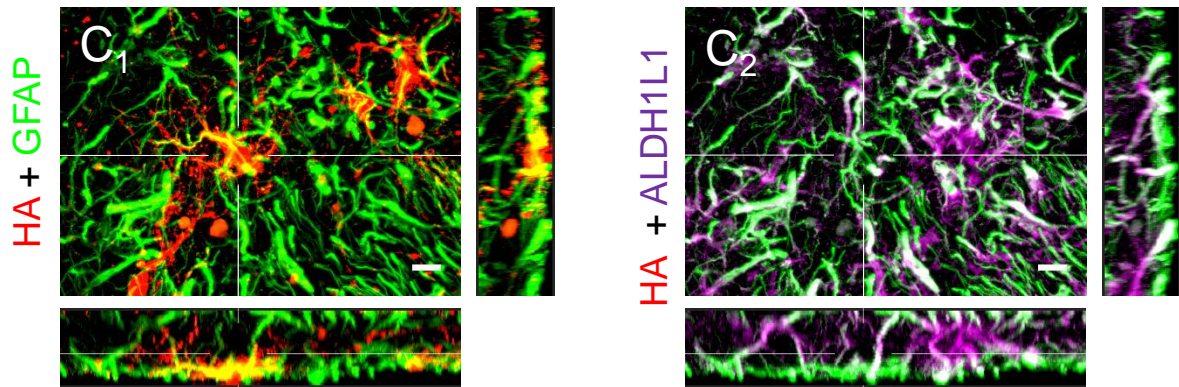
HA + GFAP + ALDH1L1



HA + S100β

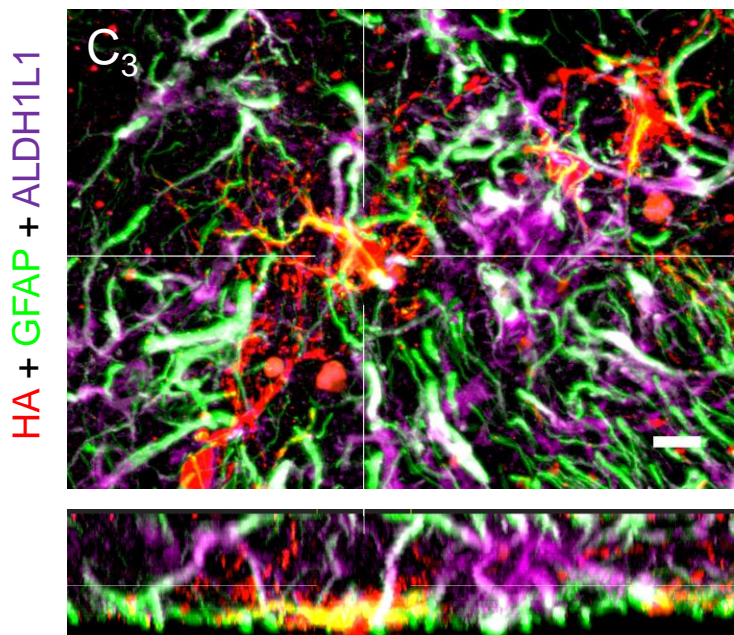
HA + GFAP

HA + GFAP + S100β



HA + GFAP

HA + ALDH1L1



HA + GFAP + ALDH1L1

Figure 10: The progeny of transplanted NSPC do not express markers of mature astrocytes at 4 weeks but do interact directly with host mature astrocytes. A) Immunohistochemical image of HA positive cells intermingling with host astrocytes (GFAP & ALDH1L1 double positive cells). HA positive cells do not express ALDH1L1 and there are discrete regions of GFAP positive cells attributed to transplanted cells that do not express ALDH1L1. **B)** Some, but not all, HA positive cells express S100 β as observed in the immunohistochemical image. White signal in **B)** indicates S100 β and HA staining co-localization. **C)** High magnification, three dimensional orthogonal projection of HA & GFAP double positive transplanted cells interacting with an ALDH1L1 & GFAP double positive host astrocyte. In **C)** yellow staining is indicative of HA and GFAP co-localization while white staining is indicative of ALDH1L1 and GFAP co-localization. Scale bars in: **A)** & **B)** are 25 μ m, **C)** is 10 μ m.

[Designated as a full page width (two column) figure]

Supplementary Information

[Click here to download Supplementary Files: Met DCH paper_ Supp info_031118_submitted.docx](#)